

1 **Microfossil evidence for trophic changes during the Eocene-Oligocene transition in the South**  
2 **Atlantic (ODP Site 1263, Walvis Ridge)**

3

4 M. Bordiga <sup>1</sup>, J. Henderiks <sup>1</sup>, F. Tori <sup>2</sup>, S. Monechi <sup>2</sup>, R. Fenero <sup>3</sup>, A. Legarda-Lisarri<sup>1,3</sup>, and E.  
5 Thomas <sup>4,5</sup>

6

7 [1] Department of Earth Sciences, Uppsala University, Villavägen 16, 752 36, Uppsala (Sweden)

8 [2] Dipartimento di Scienze della Terra, Università di Firenze, Via la Pira 4, I-50121, Florence  
9 (Italy)

10 [3] Departamento de Ciencias de la Tierra and Instituto Universitario de Investigación en Ciencias  
11 Ambientales de Aragón, Universidad de Zaragoza, Calle Pedro Cerbuna 12, E-50009, Zaragoza  
12 (Spain)

13 [4] Department of Geology and Geophysics, Yale University, New Haven, CT 06520 (USA)

14 [5] Department of Earth and Environmental Sciences, Wesleyan University, Middletown, CT 06459  
15 (USA)

16

17 Correspondence to: M. Bordiga (manuela.bordiga@geo.uu.se)

18

19 **Abstract**

20 The biotic response of calcareous nanoplankton to environmental and climatic changes during the  
21 Eocene-Oligocene transition was investigated at high resolution at Ocean Drilling Program (ODP)  
22 Site 1263 (Walvis Ridge, South East Atlantic Ocean), and compared with a lower resolution benthic  
23 foraminiferal record. During this time interval global climate, which had been warm under high  
24 levels of atmospheric CO<sub>2</sub> (pCO<sub>2</sub>) during the Eocene, transitioned into the cooler climate of the  
25 Oligocene, at overall lower pCO<sub>2</sub>. At Site 1263, the absolute nannofossil abundance (coccoliths per  
26 gram of sediment; N g<sup>-1</sup>) and the mean coccolith size decreased distinctly after the E-O boundary  
27 (EOB; 33.89 Ma), mainly due to a sharp decline in abundance of large-sized *Reticulofenestra* and  
28 *Dictyococcites*, occurring within a time-span ~47 kyr. Carbonate dissolution did not vary much  
29 across the EOB, thus the decrease in abundance and size of nannofossils may reflect an overall  
30 decrease in their export production, which could have led to variations in the food availability for  
31 benthic foraminifers.

32 The benthic foraminiferal assemblage data are consistent with a global decline in abundance of  
33 rectilinear species with complex apertures in the latest Eocene (~34.5 Ma), potentially reflecting  
34 changes in the food source, thus phytoplankton. This was followed by transient increased  
35 abundance of species indicative of seasonal delivery of food to the sea floor (*Epistominella* spp.;  
36 ~33.9-33.4 Ma), with a short peak in overall food delivery at the EOB (buliminid taxa; ~33.8 Ma).  
37 Increased abundance of *Nuttallides umbonifera* (at ~33.3 Ma) indicates the presence of more  
38 corrosive bottom waters, possibly combined arrival of less food at the sea floor after the second step  
39 of cooling (Step 2).

40 The most important changes in the calcareous nannofossil and benthic communities occurred ~120  
41 kyr after the EOB. There was no major change in nannofossil abundance or assemblage  
42 composition at Site 1263 after Step 2, although benthic foraminifera indicate more corrosive bottom  
43 waters during this time. During the onset of latest Eocene-earliest Oligocene climate change, marine  
44 phytoplankton thus showed high sensitivity to fast-changing conditions, as well as to possibly  
45 enhanced, pulsed nutrient supply, or to the crossing of a climatic threshold (e.g. pCO<sub>2</sub> decline, high-  
46 latitude cooling and changes in ocean circulation).

47

## 48 **1 Introduction**

49 The late Eocene-early Oligocene was marked by an important change in global climate and in  
50 oceanic environments, reflected in significant biotic turnover. Earth's climate was driven from a  
51 warm "greenhouse" with high pCO<sub>2</sub> during the middle Eocene through a transitional period in the  
52 late Eocene to a cold "icehouse" at low pCO<sub>2</sub> in the earliest Oligocene (e.g. Zachos et al., 2001;  
53 DeConto and Pollard, 2003; Pearson et al., 2009; Pagani et al., 2011; Zhang et al., 2013). During  
54 this climate shift, Antarctic ice sheets first reached sea level, sea level dropped, and changes  
55 occurred in ocean chemistry and plankton communities, while the calcite compensation depth  
56 (CCD) deepened rapidly, at least in the Pacific Ocean (e.g. Zachos et al., 2001; Coxall et al., 2005;  
57 Pälike et al., 2006; Coxall and Pearson, 2007; Merico et al. 2008). There is ongoing debate whether  
58 the overall cooling, starting at high latitudes in the middle Eocene while the low latitudes remained  
59 persistently warm until the end of the Eocene (Pearson et al., 2007), was mainly caused by changes  
60 in oceanic gateways (opening of Drake Passage and the Tasman gateway) leading to initiation of  
61 the Antarctic Circumpolar Current (e.g. Kennett, 1977), or by declining atmospheric CO<sub>2</sub> levels that  
62 favored ice sheet growth (e.g. DeConto and Pollard, 2003; Barker and Thomas, 2004; Katz et al.,  
63 2008; Goldner et al., 2014) in combination with specific orbital configurations (Coxall et al., 2005),  
64 or by some combination of these factors (Sijp et al., 2014). Recently, it has been proposed that the  
65 glaciation itself caused further oceanic circulation changes (Goldner et al., 2014; Ladant et al.,  
66 2014; Rugenstein et al., 2014).

67 High-resolution benthic foraminiferal  $\delta^{18}\text{O}$  records across the Eocene-Oligocene transition (EOT;  
68 ~34-33.5 Ma, Pearson et al., 2008) have shown a two-step cooling at several latitudes (e.g. Coxall et  
69 al., 2005; Katz et al., 2008; Lear et al., 2008; Coxall and Wilson, 2011; Bohaty et al., 2012). To  
70 avoid confusion with previous definitions of these two steps, we follow Pearson et al. (2008) and  
71 Bohaty et al. (2012): Step 1 is the first  $\delta^{18}\text{O}$  increase related to global cooling with a modest ice  
72 growth component, and Step 2 is the second increase in  $\delta^{18}\text{O}$  representing the major ice growth  
73 leading to a continental-scale ice sheet over Antarctica (Miller et al., 2009). Foraminifer-based  
74 geochemical studies documented the dynamics of the oceanic carbon cycle during the EOT, with an  
75 increase in benthic foraminiferal  $\delta^{13}\text{C}$  which, on kyr-time scales, could relate to an increased ratio in  
76 the burial of organic *versus* inorganic carbon (calcite) due to enhanced marine export production  
77 and/or increased preservation of organic matter (e.g. Diester-Haass, 1995; Zachos et al., 1996;  
78 Coxall and Wilson, 2011). Enhanced export production, however, may not have been global (e.g.  
79 Griffith et al., 2010; Moore et al., 2014). The  $\delta^{13}\text{C}$  shift and oceanic carbon cycle reorganization,  
80 linked to increased biological production and deepening of the CCD, have also been related to a  
81 rapid drop in pCO<sub>2</sub> (Zachos and Kump, 2005).

82 There is a strong link between late Eocene-early Oligocene climate change and the response of  
83 marine and terrestrial biota. The global cooling, with high extinction rates and ecological  
84 reorganization, affected many biological groups, including: calcifying phytoplankton  
85 (coccolithophores; e.g. Aubry, 1992; Persico and Villa, 2004; Dunkley Jones et al., 2008; Villa et  
86 al., 2008), siliceous plankton (diatoms and radiolarians; e.g. Keller, 1986; Falkowski et al., 2004),  
87 planktonic and benthic foraminifers (e.g. Coccioni et al., 1988; Thomas, 1990, 1992; Thomas and  
88 Gooday, 1996; Thomas, 2007; Pearson et al., 2008; Hayward et al., 2012), large foraminifers  
89 (*Nummulites*; e.g. Adams et al., 1986), ostracods (e.g. Benson, 1975), marine invertebrates (e.g.  
90 Dockery, 1986), and mammals (e.g. Meng and McKenna, 1998). Among the marine biota, the  
91 planktonic foraminifers experienced a synchronous extinction of five species in the Family  
92 Hantkeninidae (e.g. Coccioni et al., 1988; Coxall and Pearson, 2006), the extinction of *Turborotalia*  
93 *cerroazulensis* group and the reduction in size of the *Pseudohastigerina* lineage (Wade and Pearson,  
94 2008 and references therein). Benthic foraminifers experienced a gradual turnover, marked by an  
95 overall decline in diversity, largely due to the decline in abundance of cylindrical taxa with a  
96 complex aperture (Thomas, 2007; Hayward et al., 2012), and an increase of species which  
97 preferentially use fresh phytodetritus delivered to the seafloor in strongly seasonal pulses (e.g.  
98 Thomas, 1992; Thomas and Gooday, 1996; Pearson et al., 2008).

99 Calcareous nannoplankton assemblages underwent significant global restructuring during the EOT,  
100 although the group did not suffer extinctions exactly at the Eocene-Oligocene boundary (EOB) in  
101 contrast with planktonic foraminifers. Calcareous nannoplankton flourished and diversified during  
102 the warm-oligotrophic Eocene, with species diversity at maximum during the early-middle Eocene,  
103 decreasing during the cold-eutrophic early Oligocene (Bown et al., 2004). Furthermore,  
104 coccolithophores were globally more common and widespread in the Eocene, distinctly declining in  
105 (common) occurrence since the early Oligocene (Hannisdal et al., 2012). Species diversity  
106 decreased at the expense of specialist taxa, favoring opportunistic species that were more adapted to  
107 the new environmental conditions (e.g. Persico and Villa, 2004; Dunkley Jones et al., 2008; Tori,  
108 2008). The decline in diversity of nannoplankton since the middle Eocene coincided with a  
109 diversity increase in diatoms, which eventually outcompeted the nannoplankton as the dominant  
110 phytoplankton group (e.g. Spencer-Cervato, 1999; Bown et al., 2004; Falkowski et al., 2004).

111 In addition, the late Eocene to early Oligocene decrease in the average cell size of reticulofenestrads  
112 (ancestors of modern-day alkenone producing coccolithophores *Emiliania huxleyi* and  
113 *Gephyrocapsa oceanica*) corresponds to a decline in pCO<sub>2</sub> (Henderiks and Pagani, 2008; Pagani et  
114 al., 2011). This macroevolutionary trend appears to have been global and primarily caused by the  
115 ecological decline of large reticulofenestrads species. Henderiks and Pagani (2008) hypothesized that

116 large-celled coccolithophores were adapted to high pCO<sub>2</sub> and CO<sub>2(aq)</sub> conditions (late Eocene),  
117 whereas small-sized species are more competitive at lower pCO<sub>2</sub> (early Oligocene). This hypothesis  
118 has not yet been tested in detail in the fossil record. Culture experiments, however, provide  
119 evidence that elevated levels of CO<sub>2</sub> alleviate carbon-limitation in *E. huxleyi* and *G. oceanica*, and  
120 that even these small-celled, bloom-forming coccolithophores operate carbon concentrating  
121 mechanisms (CCMs) under today's natural conditions (e.g. Rost et al., 2003; Moolna and Rickaby,  
122 2012). The adaptations in algal carbon acquisition due to lower pCO<sub>2</sub> may have occurred as late as  
123 during the late Miocene (about 7-5 million years ago; Bolton and Stoll, 2013), suggesting that  
124 Paleogene coccolithophores did not (yet) operate CCMs and that diffusive uptake of CO<sub>2</sub> and  
125 growth rates were mainly determined by the volume-to-surface area of the cells.

126 To date, only few high-resolution studies describe the response of coccolithophores to  
127 environmental change along the EOT at high- (Southern Ocean; Persico and Villa, 2004; Villa et  
128 al., 2008, 2014) and low latitudes (Tanzania; Dunkley Jones et al., 2008; Fioroni et al., 2015). These  
129 studies have highlighted distinct shifts in the composition of the assemblages and decreasing in  
130 species diversity at or close to the boundary.

131 Here, we report on calcareous nannofossil and foraminiferal biotic events between 34.8-32.7 Ma at  
132 Ocean Drilling Program (ODP) Site 1263, recovered in the southeast Atlantic Ocean. In particular,  
133 we refine the shipboard biostratigraphy published in Zachos et al. (2004), including new data on  
134 planktonic foraminifers, and describe the ecological response of calcareous nanoplankton and  
135 benthic foraminifers to environmental change during the EOT. The reveal distinct fluctuations in  
136 total abundance and taxonomic composition of the calcareous nannofossil assemblages are  
137 compared to stable isotope data (Riesselman et al., 2007; Peck et al., 2010), and to benthic  
138 foraminiferal assemblage data. For the first time, estimates of the number of nannofossils per gram  
139 of dry sediment are calculated for the Eocene-Oligocene time interval to evaluate how paleo-export  
140 fluxes and food supply to the benthic community were affected. This is also the first high-resolution  
141 (<10,000 yr) record of coccolith size variations (and related changes in mean cell size, cf.  
142 Henderiks and Pagani, 2007) across the EOT.

143

## 144 **2 Material and methods**

### 145 **2.1 ODP Site 1263**

146 ODP Leg 208 Site 1263 (28°31.97'S and 2°46.77'E, Atlantic Ocean) was drilled at a water depth of  
147 2717 m on the southern flank of Walvis Ridge, an aseismic ridge west of the African coast (Fig. 1).

148 This site provides one of the most continuous sediment sequences of the lower Cenozoic in the  
149 Atlantic Ocean, and was at least 1 km above the lysocline prior to the lowering of the CCD during  
150 the EOT (Zachos et al., 2004). Foraminifer-bearing nannofossil ooze and nannofossil ooze are the  
151 dominant lithologies in the studied interval (Zachos et al., 2004).

152 The Eocene-Oligocene sediments of ODP Site 1263 generally have a high-carbonate content  
153 ( $\text{CaCO}_3$  wt%), ranging from 88 to 96% through 84.2-100.8 mcd (Riesselman et al., 2007). Only a  
154 few samples with lower values of  $\text{CaCO}_3$  (~87%) occur at 99.19 and 99.49 mcd (Riesselman et al.,  
155 2007).

156 A total of 190 samples was used for nannofossil analyses across the EOB. Two datasets, A and B,  
157 were independently produced at two laboratories and are here combined in a collaborative effort to  
158 also demonstrate whether, and how, the primary nannofossil signals are consistently detected from  
159 the same sediment cores independent from sample spacing, microscopy slide preparation and  
160 operator. Dataset A includes 114 samples from 83.19 to 101.13 meters composite depth (mcd). The  
161 sampling resolution is high across the EOB (5-10 cm), and decreases above and below it: 20-90 cm  
162 between 83.19-89.6 mcd, and 20-50 cm between 97.44-101.13 mcd. Dataset B includes 76 samples  
163 (83.59-105.02 mcd, sampling resolution of 10-50 cm). For analyses on benthic foraminiferal  
164 assemblages, 27 samples between 80.89 mcd to 109.79 mcd were used, while for planktonic  
165 foraminiferal analysis 16 samples between 93.42 and 107.29 mcd were studied (see Table S1,  
166 Supplement).

167

## 168 **2.2 Microfossil preparation and assemblage counts**

### 169 **2.2.1 Nannofossils**

170 Sample set A was prepared by weighing 5 mg of dried bulk sediment and diluting with 50 mL of  
171 buffered water. Then, 1.5 mL of well-mixed suspension was placed on a cover slip with a high-  
172 precision pipette, and the sample was dried on a hotplate at 60°C. This technique (called the “drop  
173 technique” by Bordiga et al., 2015; modified after Koch and Young, 2007) avoids selective settling  
174 effects because the suspension volume is placed evenly on a cover slip and left to settle and dry  
175 under low heat (see Bordiga et al., 2015 for details). Besides assuring slides with an even particle  
176 distribution, this preparation technique also allows calculation of the absolute coccolith abundances  
177 per gram of dry sediment ( $\text{N g}^{-1}$ ). Repeated sample preparation and counting revealed a coefficient  
178 of variation (CV) of 6-10% for absolute abundances (Bordiga et al., 2015), which is comparable to

179 other techniques (e.g. Bollmann et al., 1999; Geisen et al., 1999). The drop method also provides a  
180 good reproducibility for the relative species abundances (Bordiga et al., 2015).

181 In this study we report on both absolute ( $N\ g^{-1}$ ) and relative species abundances (%). Relative  
182 abundances are independent from sedimentological effects and estimates of sedimentation rate (e.g.  
183 Gibbs et al., 2012), but in contrast to absolute abundances %-values represent a closed-sum, as each  
184 percentage value refers to how common or rare a species is relative to other species without  
185 knowing whether a species truly increased or decreased in absolute abundance. For these reasons a  
186 comparison of both is helpful to evaluate the influence of dilution and sedimentation rate variations,  
187 and identify the real fluctuations in abundance of single species. Sample set B was prepared with  
188 the standard smear slide technique (Bown and Young, 1998), and the results are given as relative  
189 species abundances (%) only.

190 In both datasets A and B, calcareous nannofossils were examined under polarized light microscopy  
191 (LM) at 1000X magnification. At least 300 specimens were counted in each slide. Additional  
192 observations were performed on the slide to detect the occurrence of rare species, especially  
193 biostratigraphical markers. All specimens were identified at species or genus level, depending on  
194 the coccolith preservation. We used *Cyclicargolithus* spp. to group the specimens with dissolved  
195 central area that can be associated to the genus *Cyclicargolithus* but not directly to the species  
196 *Cyclicargolithus floridanus* (Fig. S1, Supplement). Taxonomy of the calcareous nannofossils  
197 follows the references contained in the web-site <http://ina.tmsoc.org/Nannotax3> (edited by Young et  
198 al., 2014). Additional taxonomical remarks are given in the Supplement. For dataset A, the number  
199 of fields of view (FOV) observed were also noted in order to calculate absolute abundances. An  
200 average of 26 FOVs ( $=0.31\ mm^2$ ) was observed along the sequence, from a minimum of 18 FOVs  
201 ( $=0.21\ mm^2$ ) to a maximum of 44 FOVs ( $=0.52\ mm^2$ ). Both datasets were used to provide  
202 biostratigraphical information: dataset A with a more detailed resolution across the EOB, and  
203 dataset B covering a longer interval below the EOB.

204

### 205 **2.2.2 Foraminifers**

206 The samples were oven-dried at 60°C, then washed over a 63  $\mu m$  sieve. The complete  $> 63\ \mu m$  size  
207 fraction was used for the study of benthic foraminifers. Taxa were generally determined at species  
208 level (Fenero et al., 2010) and relative abundances were calculated. The benthic foraminiferal  
209 studies were on the number of foraminifers in the full sample. All specimens were picked from  
210 material spread out in a picking tray, and mounted on microslides for identification, then deposited

211 in the Department of Earth Sciences, University of Zaragoza (Spain). The planktonic foraminiferal  
212 assemblages were observed in the >63 µm fraction to determine the presence of biostratigraphical  
213 markers, such as the *Turborotalia cerroazulensis* group and species of the Family Hantkeninidae.  
214 The presence or absence of tubulospines was noted (Table S1, Supplement). The reduction in size  
215 of the *Pseudohastigerina* lineage was observed by counting the number of *Pseudohastigerina micra*  
216 and *Pseudohastigerina naguewichiensis* in a total of 300 planktonic foraminifers in the 150-250 µm  
217 and 125-150 µm fractions (cf. Wade and Pearson, 2008; Table S1, Supplement).

218

## 219 **2.3 Biotic proxies**

### 220 **2.3.1 Nannofossil dissolution index and cell size estimates**

221 Sample set A was used to characterize nannofossil dissolution across the investigated interval. A  
222 coccolith dissolution index was calculated using the ratio between entire coccoliths and fragments  
223 (cf. Beaufort et al. 2007; Blaj et al., 2009; Pea, 2010). This index is indicative of the  
224 preservation/dissolution state of the nannofossil assemblages: higher values correspond to better  
225 preservation. Entire coccoliths and all fragments were counted until at least 300 entire coccoliths  
226 had been counted. Only pieces bigger than 3 µm were considered as fragments.

227 Mean coccolith and cell size estimates (volume-to-surface area ratio, V:SA; cf. Henderiks and  
228 Pagani, 2007; Henderiks, 2008) were calculated based on the relative abundance and size range (3-7  
229 µm, 7-11 µm and 11-16 µm for *Coccolithus*; 3-5 µm, 5-7 µm and 7-9 µm for all the other species)  
230 of placolith-bearing taxa (*Coccolithus*, *Cyclicargolithus*, *Dictyococcites* and *Reticulofenestra*).

231

### 232 **2.3.2 Calcareous nannofossil paleoecology**

233 The distribution of coccolithophores in sea surface waters is controlled by the availability of light,  
234 temperature, salinity and nutrient availability (e.g. Winter et al., 1994). Studies of modern and past  
235 paleogeographic distributions of coccolithophores, allow determination of (paleo)environmental  
236 tolerances of various taxa (see Table 3 in Villa et al., 2008). However, some paleoecological  
237 interpretations remain unresolved, or contradictory between different regions (see Table 3 in Villa  
238 et al., 2008). Therefore, we aimed to circumvent problems in interpretation by not tagging certain  
239 (groups of) species *a priori*, but instead investigating the behaviour within assemblages (see Section  
240 2.4) and then compare these with independent proxies (i.e. geochemical and benthic foraminiferal  
241 assemblage data).

242

### 243 **2.3.3 The $\delta^{13}\text{C}$ gradient in foraminiferal tests**

244 The difference between planktonic and benthic foraminiferal carbon isotope values ( $\Delta\delta^{13}\text{C}_{\text{p-b}}$ ) was  
245 proposed as a semi-quantitative proxy of paleoproductivity (Sarnthein and Winn 1990). It provides  
246 information about the surface to deep-water gradient in  $\delta^{13}\text{C}$  in Dissolved Inorganic Carbon (DIC),  
247 reflecting a combination of surface paleoproductivity and ocean circulation and stratification (e.g.  
248 Zhang et al., 2007; Bordiga et al., 2013). We calculated the  $\Delta\delta^{13}\text{C}_{\text{p-b}}$  using data in Riesselman et al.  
249 (2007) and Peck et al. (2010).

250

### 251 **2.3.4 Benthic foraminifers as paleoenvironmental proxies**

252 We determined the relative abundances of benthic foraminiferal taxa, and the diversity of the  
253 assemblages, expressed as the Fisher's alpha index (Hayek and Buzas, 2010). Changes in the  
254 relative abundances and diversity were used to infer changes in carbonate saturation state,  
255 oxygenation and food supply (e.g. Bremer and Lohmann, 1982; Jorissen et al., 1995, 2007; Gooday,  
256 2003; Thomas, 2007; Gooday and Jorissen, 2012).

257 The relative abundance of infaunal benthic foraminiferal taxa has been linked to a combination of  
258 oxygenation and food supply ('TROX model; Jorissen et al., 1995, 2007; Gooday, 2003), with high  
259 relative abundances reflecting a high food supply, extreme low oxygenation levels, or some  
260 combination of both. In addition, calcifying infaunal dwellers may gain an advantage over epifaunal  
261 dwellers during deep-water acidification (Foster et al., 2013). We have no sedimentological or  
262 stable isotope evidence for low oxygen conditions, and  $\text{CaCO}_3\%$  remains high over the studied  
263 interval (Riesselman et al., 2007). Therefore, we interpret a high relative abundance of the infaunal,  
264 triserial buliminids as indicative of a high, year-round food supply (Jorissen et al., 1995, 2007;  
265 Gooday, 2003). High relative abundances of phytodetritus-using taxa indicate an overall more  
266 moderate, as well as highly fluctuating (seasonally or episodically) flux of non-refractory  
267 particulate organic matter (e.g. Gooday, 2003; Jorissen et al., 2007). A high relative abundance of  
268 *Nuttallides umbonifera* indicates waters highly corrosive to  $\text{CaCO}_3$  in generally low-food supply  
269 settings (Bremer and Lohmann, 1982; Gooday, 2003).

270 Comparisons between past and recent benthic assemblages as indicators for features of deep-sea  
271 environments need careful evaluation, because Eocene deep-sea benthic foraminiferal assemblages  
272 were structured very differently from those living today, and the ecology even of living species is  
273 not well known. For instance, in the Paleogene, taxa reflecting highly seasonal or episodic

274 deposition of organic matter (phytodetritus) were generally absent or rare, increasing in relative  
275 abundance during the EOT (e.g. Thomas and Gooday, 1996; Thomas, 2007). At Walvis Ridge,  
276 these species did occur at much lower abundances during the EOT after Eocene hyperthermal event  
277 2 (Jennions et al., 2015), during the transition from early into middle Eocene (Ortiz and Thomas,  
278 2015) and during the middle Eocene climatic optimum (MECO; Boscolo-Galazzo et al., 2015).  
279 During the time interval from the early-late Eocene through the EOT their abundance thus increased  
280 overall, though episodically and with considerable fluctuations.

281 In contrast, in the Paleogene cylindrically-shaped taxa with complex apertures (called ‘Extinction  
282 Group’-taxa by Hayward et al., 2012) were common (e.g. Thomas, 2007). These taxa globally  
283 declined in abundance during the increased glaciation of the earliest Oligocene and middle Miocene  
284 to become extinct during the middle Pleistocene (Hayward et al., 2012). The geographic distribution  
285 of these extinct taxa resembles that of buliminids but differs in detail (e.g. Hayward et al., 2012).  
286 These taxa were probably infaunal, as confirmed by their  $\delta^{13}\text{C}$  values (Mancin et al., 2013). It is  
287 under debate what caused their Pleistocene extinction and decline in abundance across the EOB  
288 (Hayward et al., 2012; Mancin et al., 2013). Changes in the composition of phytoplankton, their  
289 food source, have been mentioned as a possible cause, as well as declining temperatures, increased  
290 oxygenation or viral infections (Hayward et al., 2012; Mancin et al., 2013).

291

#### 292 **2.4 Statistical treatment of the nannofossil data**

293 Relative species abundances are commonly lognormally distributed (MacArthur, 1960). To generate  
294 suitable datasets for statistical analysis, different transformations yielding Gaussian distributions  
295 must be applied, such as log transformation (e.g. Persico and Villa, 2004; Saavedra-Pellitero et al.,  
296 2010), centered log-ratio (e.g. Kucera and Malmgren, 1998; Buccianti and Esposito, 2004), arcsine  
297 (e.g. Auer et al., 2014).

298 The nannofossil species percentages were used in the statistical treatment to compare the datasets A  
299 and B. Two transformations were tested: i) log-transformation by  $\log(x+1)$ , which amplifies the  
300 importance of less abundant species, and minimizes the dominance of few abundant species (Mix et  
301 al., 1999), and ii) centered log-ratio (clr) transformation (Aitchison, 1986; Hammer and Harper,  
302 2006), which opens a closed data matrix and retains the true covariance structure of compositional  
303 data. The normal distribution of each species before and after the transformations was verified using  
304 SYSTAT 13.0 software. Datasets A and B were treated the same, but analysed independently.

305 Principal component analysis (PCA) was performed on the transformed data using the statistics  
306 software PAST (PAleontological STatistic; Hammer et al., 2001). Species with an abundance <1%  
307 in all samples were not included in the PCA. The PCA (Q-mode) was performed to identify the  
308 major loading species and to evaluate the main factors affecting the changes on fossil  
309 coccolithophore assemblages.

310 The closed-sum problem, or constant-sum constraint, may obscure true relationships among  
311 variables (Pearson, 1896). The clr transformation retains a major problem in carrying out the PCA  
312 on the covariance matrix, and the goal of keeping the most important data information with only  
313 few principal components (PCs) can fail using clr transformation in associations containing many  
314 outliers (e.g. Maronna et al., 2006), as often the case in nannofossil assemblages. To minimize the  
315 presence of outliers we worked with abundant species and groups of nannofossils, instead of with  
316 single species.

317 The PAST software was also used to calculate the Shannon Index, H, a diversity index taking into  
318 account a combination of evenness and diversity. High values indicate high evenness and/or high  
319 richness.

320

### 321 **3 Biostratigraphy**

322 The EOB at Site 1263 was tentatively placed between 83 and 110 mcd by the Leg 208 Shipboard  
323 Scientific Party (Zachos et al., 2004). Our high-resolution sampling allowed refining the position of  
324 the EOB by locating nannofossil and planktonic foraminiferal bioevents (Fig. 2; Table 1), including  
325 some bioevents not reported in Zachos et al. (2004).

326 The identified bioevents are delineated as Base (stratigraphic lowest occurrence of a taxon), Top  
327 (stratigraphic highest occurrence of a taxon), and Base common (Bc, first continuous and relatively  
328 common occurrence of a taxon) following Agnini et al. (2014). No correlation with magnetochrons  
329 was possible because the nannofossil oozes did not carry a clear signal (Zachos et al., 2004). The  
330 depths of all identified nannofossil and planktonic foraminiferal datums, together with the ages  
331 assigned to the most reliable datums as defined in Pälike et al. (2006) and Gradstein et al. (2012) are  
332 displayed in Table 1. Only one bioevent - the Top of *Isthmolithus recurvus* - is not reported in  
333 Pälike et al. (2006): thus, we adopted the age given in Lyle et al. (2002) (Table 1).

334 Based on the identified bioevents (see below for details), we documented that the studied  
335 succession spans from 32.7 Ma (Top of *I. recurvus*, Lyle et al., 2002) to 34.77 Ma (Top of  
336 *Discoaster barbadiensis*, Pälike et al., 2006). The estimated average sedimentation rate is 12

337 m/myr, close to the average value of ~10.8 m/myr in Zachos et al. (2004). In dataset A, where the  
338 sample distribution is more homogeneous, the sampling resolution is <10.000 years across the EOT  
339 (from 97.29 to 90.02 mcd).

340

### 341 **3.1 Calcareous nannofossils**

342 The results from both datasets A (higher-resolution) and B (longer time interval) render similar  
343 biostratigraphical evidence and well-constrained bioevents, especially for the rare species. Using  
344 the absolute ( $N\ g^{-1}$ ) and relative (%) abundances of both datasets, we identified nine calcareous  
345 nannofossil datums (Fig. 2; Table 1). The studied interval spans from CNE20 (pars) Zone to CNO2  
346 (pars) Zone, in the recent biozonation of Agnini et al. (2014). The bioevents include:

- 347 • Base of *Sphenolithus tribulosus*, the lowermost datum identified (at 103.11 mcd, Table 1). We  
348 detected this species at the top of CNE20 Zone (Fig. 2), slightly below the range reported by  
349 Bown and Dunkley Jones (2006), who documented it between the NP21 and NP23 Zones  
350 (biozonation of Martini, 1971) corresponding to the CNE21-CNO4 Zones (Agnini et al., 2014).  
351 At Site 1263, this species is rare and sporadic and poor preservation of the studied material  
352 compromises the identification at the species level and thus, possibly, its Base.
- 353 • Top of *Discoaster barbadiensis* and *Discoaster saipanensis*. The rosette-shaped discoasters at  
354 the bottom of the succession are usually well preserved without overgrowth (Fig. S1,  
355 Supplement). The Top of *D. barbadiensis* was not reported by the Shipboard Scientific Party  
356 (Zachos et al., 2004), and we placed this bioevent one meter below the Top of *D. saipanensis*  
357 (Fig. 2), identified by Zachos et al. (2004) two meters below our datum (Table 1). We placed the  
358 Top of *D. saipanensis* at 102.27 mcd because specimens of *D. saipanensis* had been  
359 continuously found until 102.52 mcd, although outside the count of 300 specimens (Fig. 2).  
360 These two bioevents were usually considered concurrent, but high-resolution studies (Berggren  
361 et al., 1995; Lyle et al., 2002; Tori, 2008; Blaj et al., 2009; Fioroni et al., 2015) show that they  
362 are shortly spaced. The Top of *D. saipanensis* is used to define the CNE20/21 zonal boundary.
- 363 • Base common of *Clausicoccus subdistichus*. We included *Clausicoccus obrutus* in the *C.*  
364 *subdistichus* concept following Agnini et al. (2014), although *C. obrutus* is the most abundant of  
365 the two species at Site 1263 (see Fig. S2, Supplement). The absolute abundance variations  
366 together with the relative abundance in the more detailed dataset A, identify the Bc at 96.92 mcd,  
367 ~2 m below the depth reported by the Leg 208 Shipboard Scientific Party (94.77 mcd; Table 1;  
368 Fig. 2) and ~60 cm above the observed Top of *Hantkenina* spp. and reduction in size of  
369 *Pseudohastigerina* (Fig. 2; see the foraminifer section). The Bc of *C. subdistichus* defines the

370 base of CNO1 (Agnini et al., 2014), which corresponds to the upper zone NP21 (Martini, 1971).  
371 The Bc of *C. subdistichus* (referred to as *C. obruta*) has been observed shortly after the EOB at  
372 Deep Sea Drilling Project (DSDP) Sites 522 and 523 in the SE Atlantic (Backman, 1987) - in the  
373 vicinity of Site 1263 - as well as in the Tethys Massignano GSSP and Monte Cagnero sections  
374 (Tori, 2008; Hyland et al., 2009), at high-latitude Site 1090 (Marino and Flores, 2002) and in the  
375 NW Atlantic (Norris et al., 2014).

- 376 • Base of *Chiasmolithus altus*. The rare and discontinuous presence of *C. altus* creates some bias  
377 in the detection of its Base. Moreover, *C. altus* specimens are highly affected by dissolution as  
378 their central-area is commonly completely dissolved (Fig. S1, Supplement). The Base of *C. altus*  
379 is tentatively placed at 89.4 mcd where a specimen with whole central crossbars meeting at 90°  
380 was observed (Fig. S1, Supplement). At Site 1263, the Base of *C. altus*, the youngest  
381 representative of the genus, falls inside the lower Oligocene (Zone CNO1; Fig. 2), as also  
382 documented NE Atlantic (de Kaenel and Villa, 1996) and at high-latitudes (Persico and Villa,  
383 2004; Villa et al., 2008).
- 384 • Base and Bc of *Sphenolithus akropodus*. Rare sporadic occurrence and poor preservation affect  
385 the recognition of this species, but Bc was identifiable (Fig. 2; Table 1). We tentatively placed  
386 the Base also, but just few and sporadic species were detected (Fig. 2). The Bc is consistent with  
387 the identified datum reported in de Kaenel and Villa (1996), who used this bioevent to  
388 approximate the Zone NP21/22 boundary, and the Top of *Coccolithus formosus*.
- 389 • Top of *Coccolithus formosus*. This bioevent was easily detectable, as *C. formosus* is abundant  
390 and well preserved. Its Top defines the CNO1/CNO2 zonal boundary (Fig. 2), close to the depth  
391 suggested on board ship (Table 1).
- 392 • Top of *Isthmolithus recurvus*, the highest datum identified (Fig. 2). Its abundance is low, so that  
393 its distribution becomes discontinuous towards the top of the studied interval. The 83.19 mcd  
394 depth (Table 1), 3 m above that reported by the Shipboard Scientific Party (Zachos et al., 2004),  
395 is an approximation because just one sample above the highest observed specimens of *I.*  
396 *recurvus* was analysed.

397

### 398 **3.2 Planktonic foraminifers**

399 The Eocene-Oligocene boundary (EOB; ~33.89 Ma, Gradstein et al., 2012) is denoted at its Global  
400 Stratotype Section and Point (GSSP) at Massignano in Italy by the extinction of the Family  
401 Hantkeninidae (specifically of species in the genera *Hantkenina* and *Cribrohantkenina*; Premoli  
402 Silva and Jenkins, 1993). Unless well-preserved material is available (as for e.g. the Tanzania

403 Drilling Project (TDP) sites; Pearson et al., 2008), the sensitivity of hantkeninids to fragmentation  
404 and dissolution may lead to a misplacement of its true highest occurrence. At several well-studied  
405 sites, for example ODP Site 744 (Zachos et al., 1996) and Site 1218 (Coxall et al., 2005),  
406 hantkeninids are not present. In such cases, additional planktonic foraminifer bioevents must be  
407 considered to identify and correlate the EOB between sites: i) the extinction of the *Turborotalia*  
408 *cerroazulensis* group which preceded the EOB (Berggren and Pearson, 2005; Pearson et al., 2008),  
409 and ii) the reduction in size of the *Pseudohastigerina* lineage which occurred at the EOB (Wade and  
410 Pearson, 2008 and references therein).

411 At Site 1263, planktonic foraminifers are abundant and their preservation is generally good to  
412 moderate. Samples from 109.79 to 99.97 mcd, however, contain strongly fragmented planktonic  
413 foraminifers, with non-broken specimens dominated by heavily calcified *Globigerinatheca* spp.  
414 (Zachos et al., 2004). Unfortunately, species of the hantkeninid group are not well preserved, and  
415 occur as fragments of variable size, including tubulospines and partial specimens (several  
416 chambers). Entire or partially preserved specimens of hantkeninids as well as loose tubulospines  
417 have been observed from the bottom sample (107.29 mcd) up to 97.91 mcd. No specimen of  
418 *Hantkenina* spp. nor even tubulospine were seen from 97.14 mcd upward (Table S1, Supplement).  
419 Therefore, we focused on the Top of *T. cerroazulensis* group (comprising *T. cerroazulensis*, *T.*  
420 *cocoaensis*, and *T. cunialensis*) and the size reduction of the *Pseudohastigerina* lineage,  
421 characterized as the Top of >125  $\mu\text{m}$ -sized *Pseudohastigerina micra*. These two bioevents were  
422 detected at the same depth as the Top of *Hantkenina* spp., i.e. the three bioevents all fall in between  
423 97.91 and 97.14 mcd (Fig. 2; Table S1, Supplement). Due to the lower resolution of the sampling  
424 for planktonic foraminifers than for nannofossils, the three bioevents may not be exactly coeval, but  
425 occur with that interval of less than 1 meter ( $\sim 70$  kyr). Nevertheless, we can refine the position of  
426 the EOB reported in Zachos et al. (2004), where only core catcher samples were studied, and place  
427 the EOB between 97.91 and 97.14 mcd, i.e. at 97.53 mcd (Fig. 2). This position of the EOB is in  
428 agreement with the nannofossil bioevent, Bc of *C. subdistichus*, just above that level (96.92 mcd;  
429 see Section 3.1).

430 A further confirmation of this placement of the EOB comes from the benthic foraminifer oxygen  
431 isotope data. The EOB occurs between the two main steps in  $\delta^{18}\text{O}$  characterizing the EOT cooling  
432 and glaciation at TDP Sites 12 and 17, where assemblage are pristine (Pearson et al., 2008). At Site  
433 1263, high resolution  $\delta^{18}\text{O}$  data are available only from 96 mcd up. Step 2 is identifiable at 93.4  
434 mcd, at the maximum value of benthic  $\delta^{18}\text{O}$  (Fig., 2; Riesselman et al., 2007; Peck et al., 2010).  
435 Step 1 was tentatively placed by Peck et al. (2010) at  $\sim 93.8$  mcd, but the  $\delta^{18}\text{O}$  curve does not reveal  
436 a signal of the first cooling step as clear as at Pacific Site 1218 (Coxall et al., 2005) and nearby Site

437 522 at Walvis Ridge (Zachos et al., 1996; Coxall and Wilson, 2011). We argue that Step 1 should  
438 be placed below 97.53 mcd at Site 1263, not only on the basis of the planktonic foraminiferal and  
439 nannofossil bioevents, but also by comparison with the oxygen isotope curve at Site 522, which  
440 records a complete and clear  $\delta^{18}\text{O}$  signal for the entire EOT (Fig. 2). The two sites are  
441 geographically close, and have comparable sedimentation rate across the EOT (12 m/myr at Site  
442 1263; 9 m/myr at Site 522, Hsü et al., 1984). Because Step 1 and Step 2 occur within ~4 meters at  
443 Site 522 (Zachos et al., 1996; Coxall and Wilson, 2011), we can infer that a similar pattern is  
444 present at Site 1263, placing the Step 1 between 97.5 and 98.5 mcd (Fig. 2). A  $\delta^{18}\text{O}$  signal similar to  
445 the one at Site 522, with Step 1 placed ~2 meters below the EOB, is recorded at Site 1265 on the  
446 Walvis Ridge (lower sampling resolution; sedimentation rate 5.7 m/myr; Liu et al., 2004). These  
447 evidences do not agree with the previous proposed position for Step 1 at only 40 cm below Step 2  
448 (Peck et al., 2010). More oxygen isotope analyses are necessary to definitely place Step 1 in the  
449 sediment column at Site 1263.

450

## 451 **4 Biotic responses**

### 452 **4.1 Calcareous nannofossil preservation and assemblages**

453 At ODP Site 1263 the carbonate content did not increase above the EOB (Fig. 3; Riesselman et al.,  
454 2007), in contrast to other sites, specifically in the Pacific Ocean (e.g. Salamy and Zachos, 1999;  
455 Coxall et al., 2005; Coxall and Wilson, 2011). This lack of response is probably due to the location  
456 of Site 1263 well above the lysocline since the late Eocene (Zachos et al., 2004), so that  $\text{CaCO}_3$   
457 (wt%) was and remained generally high, and was not affected by CCD deepening (Fig. 3;  
458 Riesselman et al., 2007). The deeper Site 1262, close to Site 1263, was below the lysocline before  
459 the rise in CCD, and shows a strong increase in  $\text{CaCO}_3$  (wt%) across the EOB (from ~5 to > 90%;  
460 Liu et al., 2004).

461 However, the  $\text{CaCO}_3$  (wt%) at Site 1263 does not reflect the total coccolith absolute abundance  
462 (Fig. 3). This supports that other calcifying organisms (mainly planktonic foraminifers) contributed  
463 consistently to the calcite accumulation in the sediments. To unravel the “true” contribution of each  
464 calcifying group to the accumulated  $\text{CaCO}_3$  (wt%), we need to know the total amount of carbonate  
465 produced by calcareous nanoplankton and foraminifers, which is beyond the scope of this study.

466 Although the site was above the lysocline during the studied time interval, the nannofossil and  
467 foraminiferal assemblages show signs of dissolution throughout the sequence. Dissolution may  
468 occur above the lysocline (e.g. Adler et al., 2001; de Villiers, 2005), leading to a reduction in

469 species numbers and an increase of fragmentation with depth, in both nannoplankton (e.g. Berger,  
470 1973; Milliman et al., 1999; Gibbs et al., 2004) and planktonic foraminiferal assemblages (e.g.  
471 Peterson and Prell, 1985).

472 At Site 1263 signs of dissolution were detected, in particular, in specimens of *Cyclicargolithus* (Fig.  
473 S1, Supplement) – one of the least resistant nannoplankton species (Blaj et al., 2009), but also in  
474 more robust species such as *Dictyococcites bisectus*. Despite these signs, holococcoliths and  
475 abundant small-medium sized *Cyclicargolithus* – which are prone to dissolution (Young et al.,  
476 2005; Bown et al., 2008; Blaj et al., 2009) – are present in all samples. We did not see small  
477 placoliths (<3  $\mu\text{m}$ ) at Site 1263, possibly due to dissolution, but these were not dominant in the late  
478 Eocene (e.g. Persico and Villa, 2004; Villa et al., 2008; Fioroni et al., 2015). The lack of such  
479 placoliths does not prevent the identification of the main features of the medium-large sized taxa.

480 Our coccolith dissolution index does not show any major changes across the EOT (91-98.5 mcd),  
481 but at 90.2 mcd and from 87 mcd upward nannofossil dissolution slightly increased (Fig. 3). The  
482 correlation between the dissolution index and total coccolith abundance is positive (entire interval  $r$   
483 = 0.32;  $p$ -value = 0) and stronger in the upper interval of the studied sequence ( $r$  = 0.59;  $p$ -value =  
484 0.002), but not significant across the EOB. Intervals of increased dissolution do not necessarily  
485 correspond to lower absolute abundances, so that we can infer that primary signals of the  
486 nannoplankton are preserved in the fossil assemblages at least across the EOB, with the exception  
487 of the primary presence/absence of small specimens.

488 Nannofossil diversity, as expressed in the H index, does not vary significantly across the EOB, but  
489 decrease gradually within 1.5 m above the EOB. A more distinct step-wise decrease at 90 mcd (Fig.  
490 3) reflects a community structure with fewer dominant species, possibly due to increased  
491 dissolution in this interval, and by a community structure with fewer dominant species. Actually,  
492 *Cyclicargolithus* became dominant in this interval, while large *Reticulofenestra* decreased in  
493 abundance significantly (Fig. 3). The calcareous nannofossil assemblage variations recorded in  
494 sample sets A and B are comparable despite the different sampling resolution (Figs. S2 and S3,  
495 Supplement).

496 The trends in absolute and relative abundances are very similar (Fig. S2, Supplement). Thus, we  
497 conclude that the dilution/sedimentation rates at Site 1263 were close to constant over time, and that  
498 the variations in absolute abundance were linked to biological processes. Total absolute coccolith  
499 abundances show a marked decrease ~1.5 m above the EOB (Fig. 3): within 60 cm (from 96.39 to  
500 95.79 mcd) the abundance rapidly drops by 45%, mainly driven by the loss of large-sized species,  
501 including *D. bisectus*, *Dictyococcites stavensis*, *Reticulofenestra umbilicus*, *Reticulofenestra*

502 *samodurovii*, *Reticulofenestra hillae*, and *Reticulofenestra circus* group (see taxonomical remarks in  
503 the Supplement). Among these, *D. bisectus* and *D. stavensis* constitute a significant part (up to  
504 28%) of the assemblage. The medium-sized *Reticulofenestra daviesii* also shows a decrease ~1.5 m  
505 above the EOB, contrary to what was reported at ODP Site 744 (Persico and Villa, 2004), Site 748  
506 (Villa et al., 2008), Site 711 (Fioroni et al., 2015), and Site 1090 (Pea, 2010) for the same time  
507 interval. The small-medium *Cyclicargolithus* spp. and *C. floridanus* are the most abundant species  
508 (up to 50%), and the 5-7  $\mu\text{m}$  size group is dominant. This group increases slightly from the bottom  
509 upwards, and just above the EOB it records an increase in abundance. *Coccolithus pelagicus* is  
510 another important component of the nannofossil assemblage, at a maximum abundance of 27%  
511 (Fig. 3). This species increases in abundance between 96.92-92.6 mcd, i.e. above the EOB, and then  
512 it decreases from 88 mcd upwards. *Sphenolithus* spp. does not show any marked variation at the  
513 EOB, even if this group is not very abundant. The increase of *Cyclicargolithus* and *C. pelagicus*  
514 does not coincide with the marked decrease of large reticulofenenstrids indicating that the loss of  
515 the latter group was not compensated for by other taxa. The total coccolith abundance (and export  
516 production) thus decreased above the EOB.

517 Another component of the assemblage, *Lanternithus minutus*, is generally not abundant, but peaks  
518 between 89.6 and 87.12 mcd. *Zygrabolithus bijugatus* and *Discoaster* spp. both decreased in  
519 abundance below the EOB (at 98 and 99 mcd, respectively) and higher in the section never reached  
520 abundances as high as in the upper Eocene (Fig. 3).

521

#### 522 **4.1.1 Principal component analysis**

523 Results from the PCAs performed on datasets A and B are comparable, both using the log- or clr-  
524 transformation. For dataset A, the Pearson correlation value ( $r$ ) between the components from the  
525 two transformations is 0.90 ( $p$ -value=0), confirming that the primary signals in the assemblage are  
526 reflected in the multivariate statistical analysis, as long as normal distribution of the species is  
527 maintained. We also compared the PCA results with or without the presence of the marker species,  
528 because stratigraphically-controlled species are not distributed along the entire succession, thus  
529 affecting PCA outcomes (e.g. Persico and Villa, 2004; Maiorano et al., 2013). The results obtained  
530 with and without the marker species provide similar trends for both datasets because in the studied  
531 interval the marker species are not very abundant (Fig. 4; Table S2, Supplement).

532 In the following discussion, we will focus on the PCA results and the loading species using the log-  
533 transformation for datasets A and B (Fig. 4; Tables S2 and S3, Supplement). The only two

534 significant principal components explain 50% of the total variance in dataset A, and respectively  
535 account for 36% and 14%. For dataset B the two components explain 35% (26% and 11%  
536 respectively).

537 Principal component 1 (PC1) of dataset A shows positive values below 96 mcd. A pronounced  
538 decrease occurs 1.5 m above the EOB, and from 96 mcd upwards the PC1 maintains mainly  
539 negative values (Fig. 4a). PC1 is negatively loaded by *C. obrutus*, *C. floridanus* small and medium  
540 size, and positively by *D. stavensis*, *D. bisectus*, *R. daviesii*, and *R. umbilicus* (Fig. 4a; Table S2,  
541 Supplement). The loadings of the other species are too low to be significant. The PC1 of dataset B  
542 does not record the same marked drop above the boundary, but rather a gradual decrease along the  
543 whole sequence (Fig. 4a). Although the main loading species are the same for both datasets (i.e. *C.*  
544 *obrutus*, *Cyclicargolithus* versus *D. bisectus* and *R. umbilicus*), there are some differences (Tables  
545 S2 and S3, Supplement). Specifically, the size groups of *Cyclicargolithus* do not influence PC1 in  
546 dataset B because the size subdivision was not included in the counts of that dataset. As the  
547 distribution of large versus small-medium sized species on the PCA seems to be important for both  
548 datasets, and *Cyclicargolithus* is one of the most abundant species, the lack of a detailed size  
549 grouping within this genus in dataset B might be the cause of the difference in the PC1 curves  
550 above the EOB. The higher abundances of *Discoaster* and *R. umbilicus* from the bottom up to 102  
551 mcd in dataset B could also explain some differences in the loading species between the two  
552 datasets (Tables S2 and S3, and Fig. S3, Supplement).

553 Principal component 2 (PC2) of dataset A also records an abrupt variation above the EOB (at 96  
554 mcd): the negative values at the bottom of the succession turn toward positive values above the  
555 boundary, remaining positive up to 89.95 mcd. From 90 mcd upwards, PC2 displays mainly  
556 negative values, except for a peak between 85.68-86.42 mcd (Fig. 4b). The most meaningful species  
557 loading on PC2 is *L. minutus* (negative loading). The PC2 is also loaded negatively by *D. stavensis*  
558 and *C. floridanus* (5-7  $\mu\text{m}$ ), and positively by *C. pelagicus* (3-7  $\mu\text{m}$  and 7-11  $\mu\text{m}$ ), *I. recurvus* and  
559 *Sphenolithus* spp. (Fig. 4b; Table S2, Supplement). The PC2 for dataset B shows a trend similar to  
560 that for dataset A from 98 mcd upward (Fig. 4b), but it distinctly differs in the lower part of the  
561 succession. Again, the PC2 is resolved by the same main loading species *L. minutus* versus *C.*  
562 *pelagicus*, but the relative direction (positive or negative) of the loadings is reversed between  
563 datasets A and B (Tables S2 and S3, Supplement). In particular, *L. minutus* has very strong loadings  
564 in both datasets. In dataset B, *L. minutus* has its maximum abundance in the upper Eocene interval  
565 not sampled in dataset A (Figs. S2 and S3, Supplement), likely driving the differences between the  
566 two PC2 curves below the EOB (Fig. 4b).

567 In the following discussion, we used the PCA results for dataset A (without marker species) only,  
568 because of its more even sample distribution and direct comparison to the other available  
569 nannofossil proxies, i.e. dissolution index, coccolith size distribution and absolute abundance.

570

#### 571 **4.2 Mean coccolithophore cell size variations**

572 The PC1 curve is mirrored ( $r=0.79$ ;  $p$ -value=0) by mean cell size estimates (V:SA ratio) of all  
573 medium to large-sized ( $>3 \mu\text{m}$ ) placolith-bearing coccolithophores within the assemblages and of  
574 those all ancient alkenone producers combined (i.e. *Cyclicargolithus*, *Reticulofenestra* and  
575 *Dictyococcites*; Plancq et al., 2012) (Fig. 5). Fluctuations in mean size are mainly driven by the  
576 relative abundance of the different placolith-bearing taxa and their respective size groups, rather  
577 than by intra-specific size variations. The mean V:SA ratios were higher (species with large cells  
578 were more abundant) during the latest Eocene and early Oligocene, and the size decreased (due to  
579 the loss of large species) by 8% between 96.39 to 95.79 mcd (within  $\sim 47$  kyr), which is according  
580 to our age model  $\sim 120$  kyr after the EOB.

581 The coccolith dissolution index confirms that preferential dissolution did not bias the V:SA results,  
582 as intervals of increased dissolution did not generally correspond to large V:SA ( $r = -0.12$ ). The  
583 only exception is the top, 90-90.3 mcd, interval where a high dissolution peak corresponds to an  
584 increase in mean size. In either case, the above V:SA considerations do not include small placoliths  
585 ( $<3 \mu\text{m}$ ), so that our analysis is free from any bias due to the (original) presence or absence of this  
586 most dissolution-prone group.

587

#### 588 **4.3 Benthic foraminiferal assemblage**

589 Benthic foraminifers show partial dissolution or etching, especially between 94.42 mcd and 109.79  
590 mcd, but are generally well preserved, i.e. sufficient for determination at species level (Fenero et al.,  
591 2010). The low-resolution data on benthic foraminifers show that the diversity of the assemblages  
592 (Fisher's alpha index curve; Fig. 6) started to decline in the late Eocene ( $\sim 34.5$  Ma; 102.79 mcd),  
593 reached its lowest values just below the EOB, then slowly recovered, but never to its Eocene values  
594 (Fenero et al., 2010). The decline in diversity was due in part to a decline in relative abundance of  
595 the generally rare but species-rich group of rectilinear species with complex apertures ('extinction  
596 group' species). Such a decline is observed globally at the end of the Eocene (Thomas, 2007;  
597 Hayward et al., 2012). The declining diversity (decreased evenness) was also due to a transient  
598 increase in abundance of species indicative of seasonal delivery of food to the sea floor

599 (phytodetritus species, mainly *Epistominella* spp.; ~33.9-33.4 Ma; 97.91-91.91 mcd), with a short  
600 peak in overall, year-round food delivery above the EOB (buliminid taxa; ~33.8 Ma; 96.41-96.27  
601 mcd). From ~3 meter above Step 2 (~33.3 Ma; 90.41 mcd) up, the abundance of *N. umbonifera*, an  
602 indicator of carbonate corrosive bottom waters, increased. Due to this evidence for dissolution,  
603 benthic foraminiferal accumulation rates cannot be used to estimate food supply quantitatively and  
604 reliably throughout the studied interval.

605 Evidence for effects of dissolution on benthic foraminiferal assemblages is seen in the interval  
606 where *N. umbonifera* is common, but not in the interval with peak abundance of phytodetritus  
607 species (thin-walled, solution-sensitive species), and the interval where buliminids peak. These  
608 intervals are also not recognized as influenced by carbonate corrosivity in the pore waters  
609 (Riesselman et al., 2007). Thus, we conclude that the increased percentage of infaunal taxa is, in  
610 this studied section, not due to dissolution, although such an effect is seen in sections with much  
611 more severe dissolution effects, such as the Paleocene-Eocene interval of ocean acidification  
612 (Foster et al., 2013). Increased abundance of buliminid taxa (though not of phytodetritus taxa) could  
613 possibly result from lowered oxygen conditions in bottom or pore waters (e.g. Jorissen et al., 2007).  
614 However, there are no indications in the sediment of low oxygen conditions (e.g. lamination), and  
615 the overall benthic assemblage does not indicate low oxygen conditions (e.g. the diversity is too  
616 high).

617

## 618 **5 Discussion**

### 619 **5.1 Nannoplankton abundance and cell size decrease after the EOB**

620 The distinct variation in nannoplankton abundance and average size of medium to large placoliths  
621 above the EOB at Site 1263 cannot be explained by dissolution – which would affect smaller  
622 coccoliths preferentially and lead to an increase of the mean size of the whole assemblage, opposite  
623 to what is observed. It can also not be explained by a change in species diversity, but is mainly  
624 linked to changes in community structure (Fig. 3). The drop in total nannofossil abundance (Fig. 3)  
625 and mean cell size (Fig. 5) is mainly driven by the decrease in abundance of large *Reticulofenestra*  
626 and *Dictyococcites* 1.5 m (~120 kyr) above the EOB. The mean V:SA estimates for all ancient  
627 alkenone producers combined (i.e. *Cyclicargolithus*, *Reticulofenestra* and *Dictyococcites*; Planq et  
628 al., 2012) tightly overlap (Fig. 5) with biometric data of the same group in the Equatorial Atlantic  
629 (Ceara Rise, ODP Sites 925 and 929; Pagani et al., 2011; Zhang et al., 2013), while the mean size  
630 estimates for combined *Reticulofenestra* and *Dictyococcites* remained relatively stable and coincide

631 with mean values measured at ODP Site 1090 in the Subantarctic Atlantic, where *Cyclicargolithus*  
632 spp. were not present and assemblages are likely severely affected by dissolution (Pea, 2010; Pagani  
633 et al., 2011). This highlights that the observed patterns in average placolith size at Site 1263 are  
634 driven by the decrease in abundance, rather than (intra-specific) size variations of *Reticulofenestra*  
635 and *Dictyococcites*.

636 The assemblages also illustrate the mid-latitude location of Site 1263, hosting both “subantarctic”  
637 and “equatorial” taxa. A striking correspondence between the mean V:SA of ancient alkenone  
638 producers at Site 1263 and Sites 929 and 925 (Fig. 5) would suggest more affinity with tropical  
639 assemblages than with high-latitude ones, south of the Subtropical Convergence (STF). The  
640 abundance patterns of the larger reticulofenestrids, however, are more similar to those at Southern  
641 Ocean sites (Persico and Villa, 2004; Villa et al., 2008). The mid-latitude Site 1263 thus probably  
642 records paleobiogeographic patterns in the nannofossil assemblage intermediate between those in  
643 equatorial-tropical and subantarctic regions.

644 The coccolith size-shift and the decreased abundance of large reticulofenestrids after the EOB may  
645 be related to different bio-limiting factors. Under growth-limiting environmental conditions,  
646 phytoplankton (coccolithophores) with small cell volume-to-surface area ratios may outcompete  
647 larger cells due to lower resource requirements (lower C, P and N cell quota) and generally higher  
648 growth rates (e.g. Daniels et al., 2014). A change in overall nutrient regime, such as in coastal  
649 upwelling *versus* oligotrophic, stratified gyre systems, may also cause a shift in opportunistic *versus*  
650 specialist taxa (e.g. Falkowski et al., 2004; Dunkley Jones et al., 2008; Henderiks et al., 2012). The  
651 16-37% absolute abundance declines of the reticulofenestrid species *R. umbilicus*, *R. samodurovii*  
652 *R. hillae* and *R. circus* group (Figs. 3 and S2, Supplement), are strong indications that these large-  
653 celled coccolithophores were at a competitive disadvantage already during or shortly after the EOB.  
654 Earlier biometric studies of reticulofenestrid coccoliths point to a similar scenario (Fig. 5),  
655 postulating that the macroevolutionary size decrease reflects the long-term decline in pCO<sub>2</sub>  
656 (Henderiks and Pagani, 2008; Pagani et al. 2011; Hannisdal et al., 2012). High CO<sub>2</sub> availability  
657 during the late Eocene could have supported high diffusive CO<sub>2</sub>-uptake rates and photosynthesis  
658 even in the largest cells, assuming that Paleogene coccolithophores had no or inefficient CO<sub>2</sub>-  
659 concentrating mechanism, similar to modern species today (Rost et al., 2003; Bolton and Stoll,  
660 2013), and due to the fact that RUBISCO specificity for CO<sub>2</sub> increases at higher CO<sub>2</sub> levels  
661 (Giordano et al., 2005).

662 Available paleo-pCO<sub>2</sub> proxy reconstructions from Equatorial regions (Pearson et al., 2009; Pagani  
663 et al., 2011; Zhang et al., 2013) indicate a transient decrease in pCO<sub>2</sub> across the studied interval,

664 rather than a distinct drop in pCO<sub>2</sub> after the EOB, which appears to be supported by our high-  
665 resolution assemblage (PC1) and mean V:SA time series (Fig. 5). The paleo-pCO<sub>2</sub> proxy data,  
666 however, are at much lower time resolution, based on a range of geochemical proxies and  
667 assumptions (Pearson et al., 2009; Pagani et al., 2011; Zhang et al., 2013). Therefore they may not  
668 record the drop in pCO<sub>2</sub> as accurately as our comparative analysis would require. The range of  
669 estimated pCO<sub>2</sub> values is fairly wide: mean values are 940 ppmv before the EOB (standard  
670 deviation range 740-1260 ppmv) and 780 ppmv after the boundary (s.d. range 530-1230 ppmv)  
671 (Pearson et al., 2009; Pagani et al., 2011; Zhang et al., 2013; Fig. 5).

672 Possibly, shortly after the EOB a threshold level in pCO<sub>2</sub> was reached, below which large  
673 reticulofenestrads became limited in their diffusive CO<sub>2</sub>-uptake, or other, fast-changing (a)biotic  
674 environmental factors limited the ecological success of this group. On million-year time scales,  
675 atmospheric CO<sub>2</sub> levels appear to have influenced coccolithophore macroevolution more than  
676 related long-term changes in temperature, sea level, ocean circulation or global carbon cycling  
677 (Hannisdal et al., 2012). Between biotic and abiotic factors, the latter (i.e. nutrient supply,  
678 temperature, salinity, etc.) are deemed to be dominant (Benton, 2009), and may have led to a more  
679 successful adaptation of the smaller taxa at the expense of large ones (see discussion below, Section  
680 5.2).

681 This would not exclude a transient, long-term pCO<sub>2</sub> forcing on coccolithophore evolution  
682 (Hannisdal et al., 2012). Interestingly, the decline of large *R. umbilicus* occurred earlier at Site 1263  
683 (~33.8 Ma) than at higher latitudes in the Southern Ocean (~33.3 Ma at Site 689, Persico and Villa,  
684 2004; ~33.5 Ma at Site 748, Villa et al., 2008). A similar pattern is documented in the timing of its  
685 subsequent extinction, occurring earlier at low- and mid-latitudes (32.02 Ma; Pälike et al., 2006)  
686 and later at high latitudes (31.35 Ma; Gradstein et al., 2012). Henderiks and Pagani (2008)  
687 suggested that the generally higher content of CO<sub>2</sub> in polar waters may have sustained *R. umbilicus*  
688 populations after it had long disappeared from the tropics.

689

## 690 **5.2 Paleoproductivity at Site 1263: nannoplankton and benthic foraminifer signals**

691 At Site 1263, no other phytoplankton than calcareous nannoplankton was detected, and diatoms  
692 were absent in coeval sediments at near-by DSDP Walvis Ridge Sites 522-529 (Hsü et al., 1984;  
693 Moore et al., 1984). Therefore, our inferences of paleo-primary productivity and export production  
694 are based on the nannoplankton and benthic foraminiferal assemblages.

695 PC2 of the calcareous nannoplankton analysis could be correlated with paleoproductivity and total  
696 water column stratification. The strongest negative loading on PC2 is the holococcolith *L. minutus*  
697 (Fig. 4b; Table S1, Supplement). In modern phytoplankton, the holococcolith-bearing life stages  
698 proliferate under oligotrophic conditions (e.g. Winter et al., 1994). Moreover, holococcoliths such  
699 as *L. minutus* and *Z. bijugatus* are quite robust (Dunkley Jones et al., 2008), so that dissolution is  
700 unlikely to affect their distribution.

701 The positive loadings on PC2 are the species *C. pelagicus*, *I. recurvus* and *Sphenolithus* spp. A high  
702 abundance of *C. pelagicus* has often been considered as indicative for warm-to-temperate  
703 temperatures at high-latitudes (e.g. Wei and Wise, 1990; Persico and Villa, 2004; Villa et al., 2008).  
704 In the modern oceans, *C. pelagicus* seems to be restricted to temperate-to-cool water, high-nutrient  
705 conditions (e.g. Cachao and Moita, 2000; Boeckel et al., 2006), but during the Paleogene it was  
706 cosmopolitan (Haq and Lohmann, 1976). The paleoecological preferences of *Sphenolithus* are still  
707 controversial, but it has been related to oligotrophic conditions inferring a major nutrient control  
708 rather than temperature control on this species during the Paleocene-Eocene thermal maximum  
709 (PETM; Agnini et al., 2006) and the EOT (Villa et al., 2008). Increased abundances of *Sphenolithus*  
710 have been also related to high-productivity intervals in the early Oligocene (Wade and Pälike, 2004)  
711 and across the EOT (Dunkley Jones et al., 2008).

712 We compared PC2 with the proxy for regional paleoproductivity  $\Delta\delta^{13}\text{C}_{\text{P-B}}$  (Fig. 6), with lower  
713 values corresponding to lower productivity and/or higher stratification.  $\Delta\delta^{13}\text{C}_{\text{P-B}}$  data are not  
714 available for the interval below 96 mcd (upper Eocene-lower Oligocene), but lower  
715 paleoproductivity in general corresponds to negative loadings on PC2, and vice versa. The  
716 correlation coefficient between the two curves is 0.33 ( $p$ -value = 0.05), i.e. a significant but not very  
717 strong correlation, possibly due to the lower number of stable isotope data points than nannofossil  
718 data points. We infer that PC2 probably reflects lower productivity during the latest Eocene, with  
719 both PC2 and  $\Delta\delta^{13}\text{C}_{\text{P-B}}$  curves showing higher productivity within the EOB and the onset of Step 2  
720 (Fig. 6). In particular, PC2 records a longer interval of positive loadings (higher productivity) after  
721 the EOB, and an initial decrease corresponding to the highest peak in  $\delta^{18}\text{O}$  (at ~93 mcd; ~33.5 Ma),  
722 as recorded also by  $\Delta\delta^{13}\text{C}_{\text{P-B}}$ . According to the  $\Delta\delta^{13}\text{C}_{\text{P-B}}$ , paleoproductivity remained constant above  
723 90 mcd upward, and lower than below Step 2. The different trend in PC2 from 90 mcd upward may  
724 be related to increased nannofossil dissolution, in particular above 87 mcd. The increase of  
725 dissolution is confirmed by the increased abundance of the benthic foraminifer species *N.*  
726 *umbonifera*, indicative of more corrosive bottom waters, and the intensified dissolution interval  
727 recorded by the coccolith dissolution index (compare Figs. 3 and 6).

728 The benthic foraminiferal assemblage confirms the above interpretation of the PC2, adding  
729 information on the nature of the supply of organic matter to the seafloor, i.e. export productivity  
730 (Fig. 6). The increase in abundance of the phytodetritus-using species across the EOB indicates an  
731 increase in seasonality of food delivery to the seafloor, correlated to the interval with positive scores  
732 on PC2 (Fig. 6). The interval was interrupted by a short period of increased productivity across the  
733 EOB (as showed by the peak in the buliminid species curve at 96.27 mcd; Fig. 6), indicating high,  
734 less seasonally interrupted food supply. Seafloor conditions changed after Step 2, when the high  
735 abundance of *N. umbonifera* and the decrease of phytodetritus and buliminid species indicate more  
736 corrosive bottom waters, possibly combined with less food arriving at the sea floor and a less  
737 pronounced seasonality (Fig. 6).

738 Variations in nutrient supply to the photic zone, as reflected in nannofossil, is a factor that could  
739 possibly have combined with the declining pCO<sub>2</sub> to cause the decrease in the mean coccolith size  
740 after the EOB. The transient higher availability of nutrients between the EOB and the onset of Step  
741 2 (~330 kyr), may have given small opportunistic nanoplankton species a competitive advantage  
742 over large specialist species after this time. The decrease of mean cell size (less biomass per  
743 individual) and overall decrease in nannofossil abundance could have led to less available organic  
744 matter or less efficient ballasting of organic matter during transport to the sea floor and, less food  
745 for the benthic foraminifers. If the smaller size led to decreased efficiency in ballasting, the time of  
746 transport from surface to the sea floor could have increased, making remineralization more efficient  
747 despite the declining temperatures. Ecosystem structure is the main determinant of efficiency of  
748 transfer of organic matter to the sea floor (e.g. Henson et al., 2012), and such important changes as  
749 observed in the nannofossil assemblages could have strongly impacted transfer of food to the  
750 seafloor, hence benthic foraminiferal assemblages, and influenced the decline in ‘Extinction Group’  
751 species (Hayward et al., 2012; Mancin et al., 2013).

752 Possibly, climate-driven instability of the water column within 330 kyr after the EOB favoured  
753 seasonal or episodic upwelling, thus primary productivity in this area, which may also be reflected  
754 by the (slightly) increasing trends in absolute abundance of (medium-sized) *Cyclicargolithus* spp.,  
755 *C. pelagicus* and *Sphenolithus* spp. (Fig. 3). After the major peak in  $\delta^{18}\text{O}$  (Step 2) a more stable  
756 system may have allowed the proliferation of more oligotrophic taxa, including holococcoliths, and  
757 the establishment of more oligotrophic, stable environmental conditions (Fig. 6).

758 Previous studies documented an increase in primary productivity during the late Eocene-early  
759 Oligocene, in particular in the Southern Ocean (e.g. Diester-Haass, 1995; Diester-Haass and Zahn,  
760 1996; Salamy and Zachos, 1999; Persico and Villa, 2004; Schumacher and Lazarus, 2004;

761 Anderson and Delaney, 2005). At tropical latitudes, both transient increases (equatorial Atlantic;  
762 Diester-Haass and Zachos, 2003) and decreases (e.g. Griffith et al., 2010; Moore et al., 2014) in  
763 paleoproductivity have been recorded during the early Oligocene, with a sharp drop in the export  
764 productivity during the early Oligocene at ~33.7 Ma (Moore et al., 2014), similar to what we  
765 observed in the SE Atlantic. Schumacher and Lazarus (2004) did not record a significant shift of  
766 paleoproductivity after the EOB in equatorial oceans, but noted a decrease in the early Oligocene  
767 (after 31 Ma). An increase in seasonality after the EOB, similar to the one we recorded at mid-  
768 latitudinal Site 1263, was documented at Site 689 in Southern Ocean (Schumacher and Lazarus,  
769 2004), while seasonality increased just before Step 2 at northern high latitudes (Eldrett et al., 2009).

770

### 771 **5.3 Timing and possible causes of the biotic response at the EOB**

772 Marine faunal and floral extinctions and community changes were coeval with the climatic  
773 deterioration during the late Eocene-early Oligocene (e.g. Adams et al., 1986; Coccioni, 1988;  
774 Berggren and Pearson, 2005; Dunkley Jones et al., 2008; Pearson et al., 2008; Tori, 2008; Villa et  
775 al., 2008, 2014). At ODP Site 1263, we see close correspondence between marked changes in the  
776 nannoplankton assemblages (i.e. nannofossil abundance and coccolith size decrease) and the  
777 benthic foraminiferal assemblages. The nannoplankton did not suffer significant extinctions at the  
778 EOB as the planktonic foraminiferal assemblage did, but the change in the community was as fast  
779 as extinction events (which occur within 10-100 kyr; Gibbs et al., 2005; Raffi et al., 2006), taking  
780 place within ~47 kyr.

781 The main shifts in the nannoplanktonic community occurred during the EOT climatic transition,  
782 ~250 kyr after the Step 1, and ~120 kyr after the EOB, but pre-dated the major cooling and increase  
783 in Antarctic ice sheet volume (i.e. Step 2) by about 200 kyr. Therefore, nannofossil assemblages  
784 prove to be sensitive and accurate tools to investigate climate thresholds and the early impacts of  
785 climate change on biotic systems.

786 Benthic foraminiferal changes at Site 1263 started before the EOB, as observed at other sites  
787 (Thomas, 1990, 2007), and the faunal turnover persisted into the early Oligocene. The benthic  
788 faunas in general show a decline in abundance of rectilinear species with complex apertures,  
789 possibly linked to the decline in nannoplankton species which they may have consumed (as e.g.  
790 hypothesized by Hayward et al., 2012, Mancin et al., 2013). The increase in phytodetritus-using  
791 species was possibly linked to more episodic upwelling and thus productivity and transport to the  
792 sea floor, and potentially blooming of more opportunistic nannoplankton species. Unfortunately, the

793 lower resolution of the benthic foraminifer data compared to the nannofossil data does not allow to  
794 unravel the exact timing of the benthic fauna response during the EOT, and also does not allow  
795 exact correlation to changes in nannofossil assemblages.

796 At Site 1263 and in Southern Ocean records (Persico and Villa, 2004; Villa et al., 2008) the large  
797 reticulofenestrads declined in abundance rapidly after the EOB. Persico and Villa (2004) and Villa  
798 et al. (2008, 2014) inferred a strong influence of SST cooling on coccolithophores, and the drop in  
799 SST shortly after the EOB at high-latitudes is confirmed by a decrease of 5°C in  $U^{K'}_{37}$ -based SST  
800 (Liu et al., 2009). In contrast, at Site 1263 planktonic foraminifer Mg/Ca data record no significant  
801 change in SST at that time (Peck et al., 2010; Fig. 5), as at ODP Sites 925 and 929 (tropical western  
802 Atlantic) where  $U^{K'}_{37}$ -based SSTs show no significant cooling (Liu et al., 2009; Fig. 5). Fairly  
803 stable SSTs were also documented in the tropics, using Mg/Ca-based SST reconstructions (Lear et  
804 al., 2008). The temperatures at mid-latitudinal Site 1263 thus may have been stable, like those in the  
805 tropics, rather than cooling, as inferred for high latitudes in the Southern Ocean (e.g. Persico and  
806 Villa, 2004; Villa et al., 2008; Liu et al., 2009; Villa et al., 2014).

807 If this is true, SST may not have been the main environmental factor affecting the nannoplankton  
808 assemblages at Site 1263 after the EOB. Andruseit et al. (2003) documented that temperature  
809 changes may be of less importance for modern coccolithophores in tropical-subtropical regions, but  
810 the lower temperature at high latitudes can approach the vital limits for coccolithophores (Baumann  
811 et al., 1997), and become important as a bio-limiting factor.

812 Changes in the phytoplankton community could be related to a global influence of declining pCO<sub>2</sub>.  
813 Unfortunately the estimates from alkenone- and boron isotopes lack the resolution to unravel the  
814 variation across and after the EOB (Fig. 5) in detail, and leave open the possibility that pCO<sub>2</sub> falling  
815 below a certain threshold-level could have played a role in driving the reorganization in the  
816 nannoplankton community. Alternatively, our combined biotic and geochemical proxy data (i.e.  
817 nannofossil and benthic foraminiferal assemblages, and  $\Delta\delta^{13}C_{P-B}$ ) suggest an increase in nutrient  
818 and food supply just after the EOB (Fig. 6), which would have favored opportunistic taxa over low-  
819 nutrient selected, specialist species. Most large reticulofenestrads (except *R. hillae* and *R. circus*  
820 group) never recovered to previous abundances, despite a return to more stratified conditions after  
821 Step 2. It is unlikely that increased dissolution above 87 mcd (33 Ma) explains the loss of large,  
822 heavily calcified taxa, but the decrease in size of coccoliths may have also have led to enhanced  
823 remineralization of organic matter and less food supply to the benthic communities.

824 There appears to be a latitudinal gradient in the timing of nannofossil abundance decreases. The  
825 total abundance decreases were first detected in the Southern Ocean (late Eocene; Persico and Villa,

826 2004), then at mid-latitude (after the EOB; this study), and finally at the equator (after Step 2, as  
827 inferred from a decrease in nannofossil species diversity at Tanzanian sites; Dunkley Jones et al.,  
828 2008). This observation may suggest a direct temperature effect on nannoplankton abundance since  
829 nannofossil floras reflect the pattern of cooling, which started and was most pronounced at high  
830 latitudes. On the other hand, high-latitude cooling may have impacted the global nutrient regimes  
831 and ocean circulation. Since regional dissolution bias may also have affected the comparison of  
832 absolute coccolith abundance, additional studies on well-preserved material will be necessary to  
833 confirm the timing and character of the response at different latitudes and in different ocean basins.  
834 Nevertheless, a meridional gradient in biotic response is expected, given the different environmental  
835 sensitivities and biogeographic ranges of different phytoplankton species (e.g. Wei and Wise, 1990;  
836 Monechi et al., 2000; Persico and Villa, 2004; Villa et al., 2008), and the diachroneity of the onset  
837 of cooling (Pearson et al., 2008).

838

## 839 **6 Conclusions**

840 High-resolution analyses of the calcareous nannofossil and foraminiferal assemblages refine the  
841 biostratigraphy at ODP Site 1263 (Walvis Ridge), and demonstrate distinct assemblage and  
842 abundance changes in marine biota across the Eocene-Oligocene transition. The biotic response of  
843 calcareous nannoplankton was very rapid (~47 kyr), following the EOB by ~120 kyr and pre-dating  
844 the climatic Step 2 event by 200 kyr.

845 The ecological success of smaller-sized coccolithophore species *versus* the drastic decrease of large  
846 reticulofenestrads, and the overall decrease of nannoplankton productivity after the EOB likely  
847 affected the benthic foraminiferal community (e.g. decrease in rectilinear species due to changes in  
848 nannoplankton floras), with increased seasonality driving the transient increased abundance of  
849 phytodetritus-using species. After Step 2 and in particular after 33.3 Ma, both nannoplankton and  
850 benthic records at Site 1263 were affected by intensified dissolution and corrosivity of bottom  
851 waters.

852 We conclude that the planktonic community reacted to fast-changing environmental conditions,  
853 possibly seasonally increased nutrient supply to the photic zone, global cooling or lowered CO<sub>2</sub>-  
854 availability, and/or the crossing of a threshold-level in the longer-term climate and environmental  
855 changes suggested by available proxy data, such as the transient *p*CO<sub>2</sub> decline during the late  
856 Eocene-early Oligocene.

857

858 **Supplement data file contains:** Table S1 (planktonic foraminiferal marker species); Tables S2 and  
859 S3 (loading species for datasets A and B); taxonomic remarks; Fig. S1 (plate of main species); Figs.  
860 S2 and S3 (plotted curves of all the distinguished species in datasets A and B).

861

## 862 **Acknowledgments**

863 The authors are grateful to the International Ocean Discovery Program (IODP) core repository in  
864 Bremen for providing samples for this research. The ODP (now IODP) was sponsored by the US  
865 National Science Foundation and participating countries under management of the Joint  
866 Oceanographic Institutions (JOI), Inc. We are thankful to Tom Dunkley Jones, Giuliana Villa and  
867 an anonymous reviewer for their constructive suggestions. We also thank Paul Pearson for his  
868 helpful comments. The project was financially supported by the Swedish Research Council (VR  
869 grant 2011-4866 to J.H.), by MIUR-PRIN grant 2010X3PP8J 005 (to S.M.), and by Spanish  
870 Ministry of Science and Technology (FEDER funds) Project CGL2011-23077 (grant BES-2012-  
871 058945 to A.L.). E.T. acknowledges the Geological Society of America and the Leverhulme  
872 Foundation (UK) for research support. We are grateful to Davide Persico and Nicolàs Campione for  
873 discussions on the statistical approach, and to Helen Coxall for helpful suggestions on the oxygen  
874 isotope stratigraphy.

875

## 876 **References**

- 877 Adams, C. G., Butterlin, J., and Samanta, B. K.: Larger foraminifera and events at the Eocene-  
878 Oligocene boundary in the Indo–West Pacific region, in: Terminal Eocene Events, edited by:  
879 Pomerol, C. and Premoli Silva, I., Elsevier, Amsterdam, 237–252, 1986.
- 880 Adler, M., Hensen, C., Wenzhöfer, F., Pfeifer, K., and Schulz, H. D.: Modelling of calcite  
881 dissolution by oxic respiration in supralysoclinal deep-sea sediments, *Mar. Geol.*, 177, 167–189,  
882 2001.
- 883 Agnini, C., Fornaciari, E., Rio, D., Tateo, F., Backman, J., and Giusberti, L.: Responses of  
884 calcareous nannofossil assemblages, mineralogy and geochemistry to the environmental  
885 perturbations across the Paleocene/ Eocene boundary in the Venetian Pre-Alps, *Mar.*  
886 *Micropaleontol.*, 63, 19–38, 2006.
- 887 Agnini, C., Fornaciari, E., Raffi, I., Catanzariti, R., Pälike, H., Backman, J., and Rio, D.:  
888 Biozonation and biochronology of Paleogene calcareous nannofossils from low and middle  
889 latitudes, *Newsletters on Stratigraphy*, 47, 131–181, 2014.

890 Aitchison, J.: The statistical analysis of compositional data. Chapman and Hall, London, 416 pp.,  
891 1986.

892 Anderson, L. D. and Delaney, L. M.: Middle Eocene to early Oligocene paleoceanography from the  
893 Agulhas Ridge, Southern Ocean (Ocean Drilling Program Leg 177, Site 1090), *Paleoceanography*,  
894 20, PA1013, doi:10.1029/2004PA001043, 2005.

895 Andruleit, H., Stäger, S., Rogalla, U., and Čepeck, P.: Living coccolithophores in the northern  
896 Arabian Sea: ecological tolerances and environmental control. *Mar. Micropaleontol.*, 49, 157–181,  
897 2003.

898 Aubry, M.-P.: Late Paleogene calcareous nannoplankton evolution; a tale of climatic deterioration,  
899 in: *Eocene-Oligocene Climatic and Biotic Evolution*, edited by: Prothero, D. R. and Berggren, W.  
900 A., Princeton University Press, 272–309, 1992.

901 Auer, G., Piller, W. E., and Harzhauser, M.: High-resolution calcareous nannoplankton  
902 palaeoecology as a proxy for small-scale environmental changes in the Early Miocene, *Mar.*  
903 *Micropaleontol.*, 111, 53–65, 2014.

904 Backman, J.: Quantitative calcareous nannofossil biochronology of middle Eocene through early  
905 Oligocene sediment from DSDP Sites 522 and 523, *Abhandlungen der Geologischen Bundesanstalt*,  
906 Vienna, 39, 21–31, 1987.

907 Barker, P. F. and Thomas, E.: Origin, signature and palaeoclimatic influence of the Antarctic  
908 Circumpolar Current, *Earth Science Reviews*, 66, 143–162, 2004.

909 Baumann, K.-H., Andruleit, H., Schröder-Ritzrau, A., and Samtleben, C.: Spatial and temporal  
910 dynamics of coccolithophore communities during non-production phases in the Norwegian-  
911 Greenland Sea, in: *Contributions to the Micropaleontology and Paleoceanography of the Northern*  
912 *North Atlantic*, edited by: Hass, H. C. and Kaminski, M. A., Grzybowski Foundation Special  
913 Publication, 5, 227–243, 1997.

914 Beaufort, L., Probert, I., and Buchet, N.: Effects of acidification and primary production on  
915 coccolith weight: Implications for carbonate transfer from the surface to the deep ocean, *Geochem.*  
916 *Geophys. Geosy.*, 8, 1–18, 2007.

917 Benson, R. H.: The origin of the psychrosphere as recorded in changes of deep-sea ostracode  
918 assemblages, *Lethaia*, 8, 69–83, 1975.

919 Benton, M. J.: The Red Queen and the Court Jester: species diversity and the role of biotic and  
920 abiotic factors through time, *Science*, 323, 728–732, 2009.

921 Berger, W. H.: Deep-sea carbonates: evidence for a coccolith lysocline, *Deep-Sea Research and*  
922 *Oceanographic Abstracts*, 20, 917–921, 1973.

923 Berggren, W. A. and Pearson, P. N.: A revised tropical to subtropical Paleogene planktonic  
924 foraminifera zonation, *J. Foramin. Res.*, 35, 279–298, 2005.

925 Berggren, W. A., Kent, D. V., Swisher, C. C., and Aubry, M.-P. A revised Cenozoic geochronology  
926 and chronostratigraphy, in: *Geochronology, time scales and global stratigraphic correlation*, SEPM  
927 Spec. Publ., 54, 129–212, 1995.

928 Blaj, T., Backman, J., and Raffi, I.: Late Eocene to Oligocene preservation history and  
929 biochronology of calcareous nannofossils from paleo-equatorial Pacific Ocean sediments, *Riv. Ital.*  
930 *Paleontol. S.*, 115, 67–85, 2009.

931 Boeckel, B., Baumann, K.-H., Henrich, R., and Kinkel, H.: Coccolith distribution patterns in South  
932 Atlantic and Southern Ocean surface sediments in relation to environmental gradients, *Deep-Sea*  
933 *Res. Pt. I*, 53, 1073–1099, 2006.

934 Bohaty, S. M., Zachos, J. C., and Delaney, M. L.: Foraminiferal Mg/Ca evidence for Southern  
935 Ocean cooling across the Eocene/Oligocene transition, *Earth Planet. Sc. Lett.*, 317, 251–261, 2012.

936 Bollmann, J., Brabec, B., Cortes, M., and Geisen, M.: Determination of absolute coccolith  
937 abundances in deep-sea sediments by spiking with microbeads and spraying (SMS method), *Mar.*  
938 *Micropaleontol.*, 38, 29–38, 1999.

939 Bolton, C. T. and Stoll, H.: Late Miocene threshold response of marine algae to carbon dioxide  
940 limitation, *Nature*, 500, 558–562, 2013.

941 Bordiga, M., Beaufort, L., Cobianchi, M., Lupi, C., Mancin, N., Luciani, V., Pelosi, N., and  
942 Sprovieri, M.: Calcareous plankton and geochemistry from the ODP site 1209B in the NW Pacific  
943 Ocean (Shatsky Rise): new data to interpret calcite dissolution and paleoproductivity changes of the  
944 last 450 ka, *Palaeogeogr. Palaeoclimatol.*, 371, 93–108, 2013.

945 Bordiga, M., Bartol, M., and Henderiks, J.: Absolute nannofossil abundance estimates: Quantifying  
946 the pros and cons of different techniques, *Revue de micropaléontologie*,  
947 <http://dx.doi.org/10.1016/j.revmic.2015.05.002>, 2015.

948 Boscolo-Galazzo, F., Thomas, E., and Giusberti, L.: Benthic foraminiferal response to the Middle  
949 Eocene Climatic Optimum (MECO) in the South-Eastern Atlantic (ODP Site 1263), *Palaeogeogr.*  
950 *Palaeoclimatol.*, 417, 432–444, 2015.

951 Bown, P. R. and Dunkley Jones, T.: New Paleogene calcareous nannofossil taxa from coastal  
952 Tanzania: Tanzania Drilling Project Sites 11 to 14, *J. Nanoplankton Res.*, 28, 17–34, 2006.

953 Bown, P. R. and Young, J. R.: Techniques, in: *Calcareous Nannofossil Biostratigraphy*, edited by:  
954 Bown, P. R., Chapman and Hall, Cambridge, 16–28, 1998.

955 Bown, P. R., Lees, J. A., and Young, J. R.: Calcareous nannoplankton evolution and diversity  
956 through time, in: *Coccolithophores*, edited by: Thierstein, H., R. and Young J. R., Springer Berlin

957 Heidelberg, 481–508, 2004.

958 Bown, P. R., Dunkley Jones, T., Lees, J. A., Randell, R. D., Mizzi, J. A., Pearson, P. N., Coxall, H.  
959 K., Young, J.R., Nicholas, C. J., Karega, A., Singano, J., and Wade, B. S.: A Paleogene calcareous  
960 microfossil Konservat-Lagerstätte from the Kilwa Group of coastal Tanzania, *Geol. Soc. Am. Bull.*,  
961 120, 3–12, 2008

962 Bremer, M. L. and Lohmann, G. P.: Evidence for primary control of the distribution of certain  
963 Atlantic Ocean benthonic foraminifera by degree of carbonate saturation, *Deep-Sea Res.*, 29, 987–  
964 998, 1982.

965 Buccianti, A. and Esposito, P.: Insights into Late Quaternary calcareous nannoplankton  
966 assemblages under the theory of statistical analysis for compositional data, *Palaeogeogr. Palaeocli.*,  
967 202, 209–277, 2004.

968 Cachao, M. and Moita, M. T.: *Coccolithus pelagicus*, a productivity proxy related to moderate  
969 fronts off Western Iberia, *Mar. Micropaleontol.*, 39, 131–155, 2000.

970 Coccioni, R.: The genera *Hantkenina* and *Cribrohantkenina* (foraminifera) in the Massignano  
971 section (Ancona, Italy), in: The Eocene–Oligocene boundary in the Marche-Umbria basin (Italy),  
972 edited by: Premoli Silva, I., Coccioni, R., and Montanari, A., International Subcommission on the  
973 Paleogene Stratigraphy, Eocene Oligocene Meeting, Ancona, Spec. Publ., 2, 81–96, 1988.

974 Coxall, H. K. and Pearson, P. N.: Taxonomy, biostratigraphy, and phylogeny of the Hantkeninidae  
975 (*Clavigerinella*, *Hantkenina*, and *Cribrohantkenina*), in: Atlas of Eocene Planktonic Foraminifera,  
976 edited by: Pearson, P. N., Olsson, R. K., Huber, B. T., Hemleben, C., and Berggren, W. A.,  
977 Cushman Foundation Special Publication, 41, 216–256, 2006.

978 Coxall, H. K. and Pearson, P. N.: The Eocene-Oligocene transition, in: Deep-time perspectives on  
979 climate change: marrying the signal from computer models and biological proxies, edited by:  
980 Williams, M., et al., Geological Society (London), Micropalaeontological Society, 351–387, 2007.

981 Coxall, H. K. and Wilson, P. A.: Early Oligocene glaciation and productivity in the eastern  
982 equatorial Pacific: insights into global carbon cycling, *Paleoceanography*, 26,  
983 doi:10.1029/2010PA002021, 2011.

984 Coxall, H. K., Wilson, P. A., Pälike, H., Lear, C. H., and Backman, J.: Rapid stepwise onset of  
985 Antarctic glaciation and deeper calcite compensation in the Pacific Ocean, *Nature*, 433, 53–57,  
986 2005.

987 Daniels, C. J., Sheward, R. M., and Poulton, A. J.: Biogeochemical implications of comparative  
988 growth rates of *Emiliania huxleyi* and *Coccolithus* species, *Biogeosciences*, 11, 6915–6925,  
989 doi:10.5194/bg-11-6915-2014, 2014.

990 De Kaenel, E. and Villa, G.: Oligocene-Miocene calcareous nannofossil biostratigraphy and  
991 paleoecology from the Iberia abyssal plain, in: Proceedings ODP, Scientific Results, College  
992 Station, TX (Ocean Drilling Program), 149, 79–145, 1996.

993 De Villiers, S.: Foraminiferal shell-weight evidence for sedimentary calcite dissolution above the  
994 lysocline. *Deep-Sea Res. Pt. I*, 52, 671–680, 2005.

995 DeConto, R. M. and Pollard, D.: Rapid Cenozoic glaciation of Antarctica induced by declining  
996 atmospheric CO<sub>2</sub>, *Nature*, 421, 245–249, 2003.

997 Diester-Haass, L.: Middle Eocene to early Oligocene paleoceanography of the Antarctic Ocean  
998 (Maud Rise, ODP Leg 113, Site 689): change from low productivity to a high productivity ocean,  
999 *Palaeogeogr. Palaeocl.*, 113, 311–334, 1995.

1000 Diester-Haass, L. and Zachos, J. C.: The Eocene-Oligocene transition in the Equatorial Atlantic  
1001 (ODP Site 325), paleoproductivity increase and positive  $\delta^{13}\text{C}$  excursion, in: from greenhouse to  
1002 icehouse: the marine Eocene-Oligocene transition, Prothero, D. R., Ivany, L. C., and Nesbitt, E. A.,  
1003 Columbia University Press, New York, 397–416, 2003.

1004 Diester-Haass, L. and Zahn, R.: Eocene-Oligocene transition in the Southern Ocean: history of  
1005 water mass circulation and biological productivity, *Geology*, 24, 163–166, 1996.

1006 Dockery III, D. T.: Punctuated succession of marine mollusks in the northern Gulf Coastal Plain,  
1007 *Palaios*, 1, 582–589, 1986.

1008 Dunkley Jones, T., Bown, P. R., Pearson, P. N., Wade, B. S., Coxall, H. K., and Lear, C. H.: Major  
1009 shift in calcareous phytoplankton assemblages through the Eocene-Oligocene transition of Tanzania  
1010 and their implications for low-latitude primary production, *Paleoceanography*, 23, PA4204,  
1011 doi:10.1029/2008PA001640, 2008.

1012 Eldrett, J. S., Greenwood, D. R., Harding, I. C., and Hubber, M.: Increased seasonality through the  
1013 Eocene to Oligocene transition in northern high latitudes, *Nature*, 459, 969–973, 2009.

1014 Falkowski, P. G., Katz, M. E., Knoll, A. H., Quigg, A., Raven, J. A., Schofield, O., and Tayler, F. J.  
1015 R.: The evolution of modern eukaryotic plankton, *Science*, 305, 354–360, 2004.

1016 Fenero, R., Thomas, E., Alegret, L., and Molina, E.: Evolución paleoambiental del tránsito Eoceno-  
1017 Oligoceno en el Atlántico sur (Sondeo 1263) basada en foraminíferos bentónicos, *Geogaceta*, 49, 3–  
1018 6, 2010 (in Spanish).

1019 Fioroni, C., Villa, G., Persico, D., and Jovane, L.: Middle Eocene-Lower Oligocene calcareous  
1020 nannofossil biostratigraphy and paleoceanographic implications from Site 711 (equatorial Indian  
1021 Ocean), *Mar. Micropaleontol.*, 118, 50–62, 2015.

1022 Foster, L. C., Schmidt, D. N., Thomas, E., Arndt, S., and Ridgwell, A.: Surviving rapid climate  
1023 change in the deep sea during the Paleogene hyperthermals, *Proceedings of the National Academy*  
1024 *of Sciences*, 110, 9273–9276, 2013.

1025 Geisen, M., Bollmann, J., Herrle, J. O., Mutterlose, J., and Young, J. R.: Calibration of the random  
1026 settling technique for calculation of absolute abundances of calcareous nannoplankton,  
1027 *Micropaleontology*, 45, 437–442, 1999.

1028 Gibbs, S. J., Shackleton, N. J., and Young, J. R.: Identification of dissolution patterns in nannofossil  
1029 assemblages: a high-resolution comparison of synchronous records from Ceara Rise, ODP Leg 154,  
1030 *Paleoceanography*, 19, PA1029, doi:10.1029/2003PA000958, 2004.

1031 Gibbs, S. J., Young, J. R., Bralower, T. J., and Shackleton, N. J.: Nannofossil evolutionary events in  
1032 the mid-Pliocene: an assessment of the degree of synchrony in the extinctions of *Reticulofenestra*  
1033 *pseudoumbilicus* and *Sphenolithus abies*, *Palaeogeogr. Palaeoclimatol.*, 217, 155–172, 2005.

1034 Gibbs, S. J., Bown, P. R., Murphy, B. H., Sluijs, A., Edgar, K. M., Pälike, H., Bolton, C. T., and  
1035 Zachos, J. C.: Interactive comment on “Scaled biotic disruption during early Eocene global  
1036 warming events”, *Biogeosciences Discuss.*, 9, C618–C620, [www.biogeosciences-](http://www.biogeosciences-discuss.net/9/C618/2012/)  
1037 [discuss.net/9/C618/2012/](http://www.biogeosciences-discuss.net/9/C618/2012/), 2012.

1038 Giordano, M., Beardall, J., and Raven, A.: CO<sub>2</sub> concentrating mechanisms in algae: mechanisms,  
1039 environmental modulation, and evolution, *Annu. Rev. Plant. Biol.*, 56, 99–131, 2005.

1040 Goldner, A., Herold, N., and Huber, M.: Antarctic glaciation caused ocean circulation changes at  
1041 the Eocene–Oligocene transition, *Nature*, 511, 574–578, 2014.

1042 Gooday, A. J.: Benthic foraminifera (Protista) as tools in deep-water palaeoceanography:  
1043 environmental influences on faunal characteristics, *Adv. Mar. Biol.*, 46, 1–90, 2003.

1044 Gooday, A. J. and Jorissen, F. J.: Benthic foraminiferal biogeography: controls on global  
1045 distribution patterns in deep-water settings, *Annual Reviews of Marine Science*, 4, 237–262, 2012.

1046 Gradstein, F. M., Ogg, J. G., Schmitz, M., and Ogg, G.: *The Geologic Time Scale 2012*, Vol. 2,  
1047 Elsevier, 1144 pp., 2012.

1048 Griffith, E., Calhoun, M., Thomas, E., Averyt, K., Erhardt, A., Bralower, T., Lyle, M., Olivarez-  
1049 Lyle, A., and Paytan, A.: Export productivity and carbonate accumulation in the Pacific Basin at the  
1050 transition from greenhouse to icehouse climate (Late Eocene to Early Oligocene),  
1051 *Paleoceanography*, 25: PA3212, doi:10.1029/2010PA001932, 2010.

1052 Hammer, Ø. and Harper, D. A. T.: *Paleontological data analysis*, Blackwell, Malden, USA, 2006.

1053 Hammer, Ø., Harper, D. A. T., and Ryan, P. D.: PAST: Paleontological Statistics Software Package  
1054 for education and data analysis, *Palaeontologia Electronica*, 4, 1–9, [http://palaeo-](http://palaeo-electronica.org/2001_2001/past/issue2001_2001.htm)  
1055 [electronica.org/2001\\_2001/past/issue2001\\_2001.htm](http://palaeo-electronica.org/2001_2001/past/issue2001_2001.htm), 2001.

1056 Hannisdal, B., Henderiks, J., and Liow, L. H.: Long-term evolutionary and ecological responses of  
1057 calcifying phytoplankton to changes in atmospheric CO<sub>2</sub>, *Glob. Change Biol.*, 18, 3504–3516,  
1058 2012.

1059 Haq, B. U. and Lohmann, G. P.: Early Cenozoic calcareous nannoplankton biogeography of the  
1060 Atlantic Ocean, *Mar. Micropaleontol.*, 1, 119–194, 1976.

1061 Hayek, L.-A. C. and Buzas, M. A.: Surveying natural populations: quantitative tools for assessing  
1062 biodiversity, Columbia University Press, 590 pp., 2010.

1063 Hayward, B. W., Kawagata, S., Sabaa, A. T., Grenfell, H. R., van Kerckhoven, L., Johnson, K., and  
1064 Thomas, E.: The last global extinction (Mid-Pleistocene) of deep-sea benthic foraminifera  
1065 (*Chrysalogoniidae*, *Ellipsoidinidae*, *Glandulonodosariidae*, *Plectofrondiculariidae*,  
1066 *Pleurostomellidae*, *Stilostomellidae*), their Late Cretaceous-Cenozoic history and taxonomy.  
1067 Cushman Foundation For Foraminiferal Research, Spec. Publ., 43, 408 pp., 2012.

1068 Henderiks, J.: Coccolithophore size rules - reconstructing ancient cell geometry and cellular calcite  
1069 quota from fossil coccoliths, *Mar. Micropaleontol.*, 67, 143–154, 2008.

1070 Henderiks, J. and Pagani, M.: Refining ancient carbon dioxide estimates: significance of  
1071 coccolithophore cell size for alkenone-based *p*CO<sub>2</sub> records, *Paleoceanography*, 22, PA3202,  
1072 doi:10.1029/2006PA001399, 2007.

1073 Henderiks, J. and Pagani, M.: Coccolithophore cell size and Paleogene decline in atmospheric CO<sub>2</sub>,  
1074 *Earth Planet. Sc. Lett.*, 269, 576–584, 2008.

1075 Henderiks, J., Winter, A., Elbrächter, M., Feistel, R., van der Plas, A. K., Nausch, G., and Barlow,  
1076 R.: Environmental controls on *Emiliania huxleyi* morphotypes in the Benguela coastal upwelling  
1077 system (SE Atlantic), *Mar. Ecol. Prog. Ser.*, 448, 51–66, 2012.

1078 Henson, S. A., Sanders, R., and Madsen, E.: Global patterns in efficiency of particulate organic  
1079 carbon export and transfer to the deep ocean, *Global Biogeochem. Cy.*, 26, GB1028,  
1080 doi:10.1029/2011GB004099, 2012.

1081 Hsü, K. J., LaBrecque, J. L., Carman Jr, M. F., and Shipboard Scientific Party: Site 522, in: DSDP,  
1082 Initial Reports, College Station, TX, 73, 187–270, 1984.

1083 Hyland, E., Murphy, B., Varela, P., Marks, K., Colwell, L., Tori, F., Monechi, S., Cleaveland, L.,  
1084 Brinkhuis, H., Van Mourik, C. A., Coccioni, R., Bice, D., and Montanari, A.: Integrated  
1085 stratigraphic and astrochronologic calibration of the Eocene-Oligocene transition in the Monte  
1086 Cagnero section (northeastern Apennines, Italy): a potential parastratotype for the Massignano  
1087 global stratotype section and point (GSSP), in: *The Late Eocene Earth: Hothouse, Icehouse, and*  
1088 *Impacts*, edited by: Koeberl, C. and Montanari, A., *Geol. S. Am. S.*, 452, 303–322, 2009.

1089 Jennions, S. M., Thomas, E., Schimdt, D. N., Lunt, D., and Ridgwell, A.: Changes in benthic  
1090 ecosystems and ocean circulation in the Southeast Atlantic across Eocene Thermal Maximum 2,  
1091 *Paleoceanography*, 30, doi:10.1002/2015PA002821, 2015.

1092 Jorissen, F. J., de Stigter, H. C., and Widmark, J. G. V.: A conceptual model explaining benthic  
1093 foraminiferal microhabitats, *Mar. Micropaleontol.*, 26, 3–15, 1995.

1094 Jorissen, F. J., Fontanier, C., and Thomas, E.: Paleooceanographical proxies based on deep-sea  
1095 benthic foraminiferal assemblage characteristics, in: *Proxies in Late Cenozoic Paleooceanography:*  
1096 *Pt. 2: Biological tracers and biomarkers*, edited by: Hillaire-Marcel, C. and de Vernal, A., Elsevier,  
1097 263–326, 2007.

1098 Katz, M. E., Miller, K. G., Wright, J. D., Wade, B. S., Browning, J. V., Cramer, B. S., and  
1099 Rosenthal, Y.: Stepwise transition from the Eocene greenhouse to the Oligocene icehouse, *Nat.*  
1100 *Geosci.*, 1, 329–334, 2008.

1101 Keller, G.: Stepwise mass extinctions and impact events: Late Eocene to early Oligocene, *Mar.*  
1102 *Micropaleontol.*, 10, 267–293, 1986.

1103 Kennett, J. P.: Cenozoic evolution of Antarctic glaciation, the circum-Antarctic Ocean, and their  
1104 impact on global paleoceanography, *J. Geophys. Res.*, 82, 3843–3860, 1977.

1105 Koch, C. and Young, J. R.: A simple weighing and dilution technique for determining absolute  
1106 abundances of coccoliths from sediment samples, *Journal of Nannoplankton Research*, 29, 67–69,  
1107 2007.

1108 Kucera, M. and Malmgren, B. A.: Logratio transformation of compositional data – a resolution of  
1109 the constant sum constraint, *Mar. Micropaleontol.*, 34, 117–120, 1998.

1110 Ladant, J.-B., Donnadieu, Y., and Dumas, C.: Links between CO<sub>2</sub>, glaciation and water flow:  
1111 reconciling the Cenozoic history of the Antarctic Circumpolar Current, *Clim. Past.*, 10, 1957–1966,  
1112 2014.

1113 Lear, C. H., Bailey, T. R., Pearson, P. N., Coxall, H. K., and Rosenthal, Y.: Cooling and ice growth  
1114 across the Eocene-Oligocene transition, *Geology*, 36, 251–254, 2008.

1115 Liu, Z., Tuo, S., Zhao, Q., Cheng, X., and Huang, W.: Deep-water earliest Oligocene Glacial  
1116 Maximum (EOGM) in South Atlantic, *Chinese Sci. Bull.*, 49, 2190–2197, 2004.

1117 Liu, Z., Pagani, M., Zinniker, D., DeConto, R. M., Huber, M., Brinkhuis, H., Shah, S. R., Leckie, R.  
1118 M., and Pearson, A.: Global cooling during the Eocene-Oligocene climate transition, *Science*, 323,  
1119 1187–1190, 2009.

1120 Lyle, M., Wilson, P. A., Janecek, T. R., et al.: Leg 199 Summary, in: *Proceedings ODP, Initial*  
1121 *Reports*, College Station, TX (Ocean Drilling Program), 199, 1–87, 2002.

1122 MacArthur, R. H.: On the relative abundance of species, *Am. Nat.*, 94, 25–36, 1960.

1123 Maiorano, P., Tarantino, F., Marino, M., and De Lange, G. J.: Paleoenvironmental conditions at  
1124 Core KC01B (Ionina Sea) through MIS 13-9: evidence from calcareous nannofossil assemblages,  
1125 Quatern. Int., 288, 97–111, 2013.

1126 Mancin, N., Hayward, B. H., Trattenero, I., Cobianchi, M., and Lupi, C.: Can the morphology of  
1127 deep-sea benthic foraminifera reveal what caused their extinction during the mid-Pleistocene  
1128 Climate Transition?, Mar. Micropaleontol., 104, 53–70, 2013.

1129 Marino, M. and Flores, J. A.: Middle Eocene to early Oligocene calcareous nannofossil stratigraphy  
1130 at Leg 177 Site 1090, Mar. Micropaleontol., 45, 291–307, 2002.

1131 Maronna, R., Martin, R. D., and Yohai, V. J.: Robust statistics: Theory and methods, Wiley J., New  
1132 York, 2006.

1133 Martini, E.: Standard Tertiary and Quaternary calcareous nannoplankton zonation, Proc. 2<sup>nd</sup> Conf.  
1134 Planktonic Microfossils, Rome, 2, 739–786, 1971.

1135 Meng, J. and McKenna, M. C.: Faunal turnovers of Palaeogene mammals from the Mongolian  
1136 Plateau, Nature, 394, 364–367, 1998.

1137 Merico, A., Tyrrell, T., and Wilson, P. A.: Eocene/Oligocene ocean de-acidification linked to  
1138 Antarctic glaciation by sea-level fall, Nature 452, 979–982, 2008.

1139 Miller, K. G., Wright, J. D., Katz, M. E., Wade, B. S., Browning, J. V., Cramer, B. S., and  
1140 Rosenthal, Y.: Climate threshold at the Eocene-Oligocene transition: Antarctic ice sheet influence  
1141 on ocean circulation, Geol. Soc. Am. Spec. Pap., 452, 169–178, 2009.

1142 Milliman, J. D., Troy, P. J., Balch, W. M., Adams, A. K., Li, Y.-H., and Mackenzie, F. T.:  
1143 Biologically mediated dissolution of calcium carbonate above the chemical lysocline? Deep-Sea  
1144 Res. Pt. I, 46, 1653–1669, 1999.

1145 Mix, A. C., Morey, A. E., Pisias, N. G., and Hostetler, S. W.: Foraminiferal faunal estimates of  
1146 paleotemperature: circumventing the no-analog problem yields cool ice age tropics,  
1147 Paleoceanography, 14, 350–359, doi:10.1029/1999PA900012, 1999.

1148 Monechi, S., Buccianti, A., and Gardin, S.: Biotic signals from nannoflora across the iridium  
1149 anomaly in the upper Eocene of the Massignano section: evidence from statistical analysis, Mar.  
1150 Micropaleontol., 39, 219–237, 2000.

1151 Moolna, A. and Rickaby, R. E. M.: Interaction of the coccolithophore *Gephyrocapsa oceanica* with  
1152 its carbon environment: response to a recreated high-CO<sub>2</sub> geological past, Geobiology, 10, 72–81,  
1153 2012.

1154 Moore, T. C., Rabinowitz, P. D., et al.: Site 525-529, in: Deep Sea Drilling Project, Initial Reports,  
1155 US Government Printing Office, Washington, DC, USA, 74, 41–465, 1984.

1156 Moore, T. C., Wade, B. S., Westerhold, T., Erhardt, A., M., Coxall, H. K., Baldauf, J., and Wagner,

1157 M.: Equatorial Pacific productivity changes near the Eocene-Oligocene boundary,  
1158 *Paleoceanography*, 29, 825–844, doi:10.1002/2014PA002656, 2014.

1159 Norris, R. D., Wilson, P. A., Blum, P., and the Expedition 342 Scientists: Proceedings IODP, 342,  
1160 College Station, TX (Integrated Ocean Drilling Program), doi:10.2204/iodp.proc.342.2014, 2014.  
1161 Ocean Drilling Stratigraphic Network, Plate Tectonic Reconstruction Service:  
1162 <http://www.odsn.de/odsn/services/paleomap/paleomap.html>, last access: 10 April 2015, 2011.

1163 Ortiz, S. and Thomas, E.: Deep-sea benthic foraminiferal turnover during the early middle Eocene  
1164 transition at Walvis Ridge (SE Atlantic), *Palaeogeogr. Palaeoclimatol.*, 417, 126–136, 2015.

1165 Pagani, M., Huber, M., Liu, Z., Bohaty, S. M., Henderiks, J., Sijp, W., Krishnan, S., and DeConto,  
1166 R. M.: The role of carbon dioxide during the onset of Antarctic glaciation, *Science*, 334, 1261–  
1167 1264, 2011.

1168 Pälike, H., Norris, R. D., Herrle, J. O., Wilson, P. A., Coxall, H. K., Lear, C. H., Shackleton, N. J.,  
1169 Tripathi, A. K., and Wade, B. S.: The heartbeat of the Oligocene climate system, *Science*, 314, 1894–  
1170 1898, 2006.

1171 Pea, L.: Eocene-Oligocene paleoceanography of the subantarctic South Atlantic: calcareous  
1172 nannofossil reconstructions of temperature, nutrient, and dissolution history, Ph.D. thesis,  
1173 Department of Earth Sciences, University of Parma, Italy, 210 pp., 2010.

1174 Pearson, K.: Mathematical contributions to the theory of evolution. On a form of spurious  
1175 correlation which may arise when indices are used in the measurement of organisms, *P. R. Soc.*  
1176 *London*, 60, 489–498, 1896.

1177 Pearson, P. N., van Dogen, B. E., Nicholas, C. J., Pancost, R. D., Schouten, S., Singano, J. M., and  
1178 Wade, B. S.: Stable warm tropical climate through the Eocene Epoch, *Geology*, 35, 211–214, 2007.

1179 Pearson, P. N., McMillan, I. K., Wade, B. S., Dunkley Jones, T., Coxall, H. K., Bown, P. R., and  
1180 Lear, C. H.: Extinction and environmental change across the Eocene-Oligocene boundary in  
1181 Tanzania, *Geology*, 36, 179–182, 2008.

1182 Pearson, P. N., Gavin, L. F., and Wade, B. S.: Atmospheric carbon dioxide through the Eocene–  
1183 Oligocene climate transition, *Nature*, 461, 1110–1114, 2009.

1184 Peck, V. L., Yu, J., Kender, S., and Riesselman, C. R.: Shifting ocean carbonate chemistry during  
1185 the Eocene-Oligocene climate transition: implications for deep-ocean Mg/Ca paleothermometry,  
1186 *Paleoceanography*, 25, doi:10.1029/2009PA001906, 2010.

1187 Persico, D. and Villa, G.: Eocene-Oligocene calcareous nannofossils from Maud Rise and  
1188 Kerguelen Plateau (Antarctica): paleoecological and paleoceanographic implications, *Mar.*  
1189 *Micropaleontol.*, 52, 153–179, 2004.

1190 Peterson, L. C. and Prell, W. L.: Carbonate dissolution in recent sediments of the eastern equatorial  
1191 Indian Ocean: preservation patterns and carbonate loss above the lysocline, *Mar. Geol.*, 64, 259–  
1192 290, 1985.

1193 Plancq, J., Grossi, V., Henderiks, J., Simon, L., and Mattioli, E.: Alkenone producers during late  
1194 Oligocene–early Miocene revisited, *Paleoceanography*, 27, PA1202, doi:10.1029/2011PA002164,  
1195 2012.

1196 Premoli Silva, I. and Jenkins, D. G.: Decision on the Eocene-Oligocene boundary stratotype,  
1197 *Episodes*, 16, 379–382, 1993.

1198 Raffi, I., Backman, J., Fornaciari, E., Pälike, H., Rio, D., Lourens, L., and Hilgen, F.: A review of  
1199 calcareous nannofossil astrobiochronology encompassing the past 25 million years, *Quaternary Sci.*  
1200 *Rev.*, 25, 3113–3137, 2006.

1201 Riesselman, C. R., Dunbar, R. B., Mucciarone, D. A., and Kitasei, S. S.: High resolution stable  
1202 isotope and carbonate variability during the early Oligocene climate transition: Walvis Ridge (ODP  
1203 Site 1263), in: *Antarctica: A Keystone in a Changing World-Online Proceedings of the 10<sup>th</sup> ISAES*,  
1204 edited by: Cooper, A. K., Raymond, C. R., and the 10th ISAES Editorial Team, US Geol. Surv.,  
1205 doi:10.3133/of2007-1047.srp095, 2007.

1206 Rost, B., Riebesell, U., Burkhardt, S., and Sültemeyer, D.: Carbon acquisition of bloom-forming  
1207 marine phytoplankton, *Limnol. Oceanogr.*, 48, 55–67, 2003.

1208 Rugenstein, M., Stocchi, P., von der Heijdt, A., Dijkstra, H., and Brinkhuis, H.: Emplacement of  
1209 Antarctic ice sheet mass circumpolar ocean flow, *Global Planet. Change*, 118, 16–24, 2014.

1210 Saavedra-Pellitero, M., Flores, J. A., Baumann, K.-H., and Sierro, F. J.: Coccolith distribution  
1211 patterns in surface sediments of Equatorial and Southeastern Pacific Ocean, *Geobios*, 43, 131–149,  
1212 2010.

1213 Salamy, K. A. and Zachos, J. C.: Latest Eocene-early Oligocene climate change and Southern  
1214 Ocean fertility: inferences from sediment accumulation and stable isotope data, *Palaeogeogr.*  
1215 *Palaeocl.*, 145, 61–77, 1999.

1216 Sarnthein, M. and Winn, K.: Reconstruction of low and middle latitude export productivity, 30,000  
1217 years BP to present: implication for global carbon reservoir, in: *Climate-Ocean Interaction*, edited  
1218 by: Schlesinger, M. E., Kluwer Academic Publishers, 319–342, 1990.

1219 Schumacher, S. and Lazarus, D.: Regional differences in pelagic productivity in the late Eocene to  
1220 early Oligocene - a comparison of southern high latitudes and lower latitudes, *Palaeogeogr.*  
1221 *Palaeocl.*, 214, 243–263, 2004.

1222 Sijp, W. P., von der Heydt, A. S., Dijkstra, H. A., Flögel, S., Douglas, P. J., and Bijl, P. K.: The role  
1223 of ocean gateways on cooling climate on long time scales, *Global Planet. Change*, 119, 1–22, 2014.

1224 Spencer-Cervato, C.: The Cenozoic deep sea microfossil record: explorations of the DSDP/ODP  
1225 sample set using the Neptune Database, *Palaeontol. Electron.*, 2, 2, 270 pp., 1999.

1226 Thomas, E.: Late Cretaceous through Neogene deep-sea benthic foraminifers (Maud Rise, Weddell  
1227 Sea, Antarctica), in: *Proceedings ODP, Scientific Results*, College Station, TX (Ocean Drilling  
1228 Program), 113, 571–594, 1990.

1229 Thomas, E.: Middle Eocene - late Oligocene bathyal benthic foraminifera (Weddell Sea): faunal  
1230 changes and implications for ocean circulation, in: *Late Eocene-Oligocene climatic and biotic*  
1231 *evolution*, edited by: Prothero, D. R., and Berggren, W. A., Princeton University Press, 245–271,  
1232 1992.

1233 Thomas, E.: Cenozoic mass extinctions in the deep sea: what disturbs the largest habitat on Earth?,  
1234 in: *Large ecosystem perturbations: causes and consequences*, edited by: Monechi, S., Coccioni, R.,  
1235 and Rampino, M., *Geol. S. Am. S.*, 424, 1–23, 2007.

1236 Thomas, E. and Gooday, A. J.: Cenozoic deep-sea benthic foraminifers: tracers for changes in  
1237 oceanic productivity?, *Geology*, 24, 355–358, 1996.

1238 Tori, F.: Variabilità climatica e ciclicità nell'intervallo Eocene Oligocene: dati dai nannofossili  
1239 calcarei, Ph.D. thesis, Department of Earth Sciences, University of Florence, Italy, 222 pp., 2008 (in  
1240 Italian).

1241 Villa, G., Fioroni, C., Pea, L., Bohaty, S., and Persico, D.: Middle Eocene-late Oligocene climate  
1242 variability: calcareous nannofossil response at Kerguelen Plateau, Site 748, *Mar. Micropaleontol.*,  
1243 69, 173–192, 2008.

1244 Villa, G., Fioroni, C., Persico, D., Roberts, A. P., and Florindo, F.: Middle Eocene to Late  
1245 Oligocene Antarctic glaciation/deglaciation and Southern Ocean productivity, *Paleoceanography*,  
1246 29, 223–237, doi:10.1002/2013PA002518, 2014.

1247 Wade, B. S. and Pälike, H.: Oligocene climate dynamics, *Paleoceanography*, 19, PA4019,  
1248 doi:10.1029/2004PA001042, 2004.

1249 Wade, B. S. and Pearson, P. N.: Planktonic foraminiferal turnover, diversity fluctuations and  
1250 geochemical signals across the Eocene/Oligocene boundary in Tanzania, *Mar. Micropaleontol.*, 68,  
1251 244–255, 2008.

1252 Wei, W. and Wise, S. W.: Biogeographic gradients of middle Eocene–Oligocene calcareous  
1253 nannoplankton in the South Atlantic Ocean, *Palaeogeogr. Palaeoclimatol.*, 79, 29–61, 1990.

1254 Winter, A., Jordan, R. W., and Roth, P. H.: Biogeography of living coccolithophores in ocean  
1255 waters, in: *Coccolithophores*, edited by: Winter, A. and Siesser, W. G., 161–177, 1994.

1256 Young, J. R., Geisen, M., and Probert, I.: A review of selected aspects of coccolithophore biology  
1257 with implications for paleodiversity estimation, *Micropaleontology*, 51,267–288,  
1258 doi:10.2113/gsmicropal.51.4.267, 2005

1259 Young, J. R., Bown P.R., and Lees, J. A.: Nannotax3 website, International Nannoplankton  
1260 Association, 21 Apr. 2014, URL: <http://http://ina.tmsoc.org/Nannotax3>, last access: 21 March 2015,  
1261 2014.

1262 Zachos, J. C. and Kump, L. R.: Carbon cycle feedbacks and the initiation of Antarctic glaciation in  
1263 the earliest Oligocene, *Global Planet. Change*, 47, 51–66, 2005.

1264 Zachos, J. C., Quinn, T. M., and Salamy, K. A.: High-resolution (104 years) deep-sea foraminiferal  
1265 stable isotope records of the Eocene-Oligocene climate transition, *Paleoceanography*, 11, 251–266,  
1266 doi:10.1029/96PA00571, 1996.

1267 Zachos, J., Pagani, M., Sloan, L., Thomas, E., and Billups, K.: Trends, rhythms, and aberrations in  
1268 global climate 65 Ma to present, *Science*, 292, 686–693, 2001.

1269 Zachos, J. C., Kroon, D., Blum, P., and Shipboard Scientific Party: Site 1263, in: *Proceedings ODP,*  
1270 *Initial Reports*, College Station, TX (Ocean Drilling Program), 208, 1–87, 2004.

1271 Zhang, J., Wang, P., Li, Q., Cheng, X., Jin, H., and Zhang, S.: Western equatorial Pacific  
1272 productivity and carbonate dissolution over the last 550 kyr: foraminiferal and nannofossil evidence  
1273 from ODP Hole 807A, *Mar. Micropaleontol.*, 64, 121–140, 2007.

1274 Zhang, Y. G., Pagani, M., Liu, Z., Bohaty, S. M., and DeConto, R. M.: A 40-million-year history of  
1275 atmospheric CO<sub>2</sub>, *Philos. T. Roy. Soc. A.*, 371, 20130096, 2013.

1276

## 1277 **Table caption**

1278 **Table 1.** Calcareous nannofossil and planktonic foraminiferal (underlined) bioevents as identified in  
1279 this study (at meter composite depth, mcd), and the mcd reported by the Shipboard Scientific Party  
1280 (Zachos et al., 2004). Note that for the planktonic foraminiferal bioevents the average depth is  
1281 reported. For each bioevent, the ages available in the most recent literature are given. N.A.: not  
1282 available datum; \*: ages not included in the sedimentation rate estimate.

1283

## 1284 **Figure captions**

1285 **Figure 1.** Paleogeographic reconstruction at 33 Ma (modified from Ocean Drilling Stratigraphic  
1286 Network, Plate Tectonic Reconstruction Service,  
1287 [www.odsn.de/odsn/services/paleomap/paleomap.html](http://www.odsn.de/odsn/services/paleomap/paleomap.html)) showing location of ODP Site 1263 (black

1288 dot) on Walvis Ridge. The positions of the other sites (white squares) used for comparison and cited  
1289 in the text are also given.

1290

1291 **Figure 2.** Eocene-Oligocene stratigraphy of Site 1263 and DSDP Site 522 (Walvis Ridge). Stable  
1292 oxygen isotope stratigraphy ( $\delta^{18}\text{O}$ , ‰) DSDP Site 522 (Zachos et al., 1996) compared to that at Site  
1293 1263 (Riesselman et al., 2007). Absolute abundances of nannofossil marker species ( $\text{N g}^{-1}$ ; note  
1294  $10^7$ - $10^8$  change in scale among curves) for dataset A (grey line) and their relative percentages (%)  
1295 for datasets A (black line) and B (black dashed). A 5 pt. smoothed curve is shown for the species *C.*  
1296 *subdistichus*. Note the changes in horizontal scale among curves. Calcareous nannofossil and  
1297 planktonic foraminiferal datums are highlighted. B: Base occurrence; T: Top occurrence; Bc: Base  
1298 common occurrence.

1299

1300 **Figure 3.** Calcareous nannofossil abundance and distribution against depth (mcd) at Site 1263  
1301 (dataset A).  $\text{CaCO}_3$  (wt%; Riesselman et al., 2007), coccolith dissolution index (%), H index, and  
1302 the total absolute coccolith abundance ( $\text{N g}^{-1}$ ). Error bars indicates the standard deviation ( $\pm 1$  s.d.,  
1303 in %) of replicate counts. The absolute ( $\text{N g}^{-1}$ , black line) and relative (% , green line) abundances of  
1304 the main species constituting the assemblage are shown. For *Cyclicargolithus* spp. and *C. pelagicus*  
1305 the absolute abundances of different size groups are shown. The grey vertical bar marks an interval  
1306 of major dissolution (87 to 83 mcd). The positions of EOB and Step 2 are reported.

1307

1308 **Figure 4.** Distribution patterns of PC1 (a) and PC2 (b) obtained from the PCA for the datasets A  
1309 and B. Loadings of calcareous nannofossil taxa on the two principal components of the whole  
1310 studied succession for dataset A are reported. The shaded boxes represent the most relevant loaded  
1311 species. Shaded area: PCs (dataset A) obtained omitting the marker species in the dataset. Red line:  
1312 PCs (dataset A) obtained inserting also the marker species. The positions of EOB and Step 2 are  
1313 reported.

1314

1315 **Figure 5.** PC1 and cell-size trends during the Eocene-Oligocene at Site 1263. The average cell  
1316 V:SA ( $\mu\text{m}$ ) of all placolith-bearing species (green area), *Reticulofenestra-Dictyococcites-*  
1317 *Cyclicargolithus* (red solid line) and *Reticulofenestra-Dictyococcites* (green dotted line) are  
1318 reported. The average cell V:SA of ODP 925 (black circles; Pagani et al., 2011), DSDP 516 (white

1319 triangles; Henderiks and Pagani, 2008), DSDP 511-277 (white squares) and ODP 1090 (black  
1320 squares) from the southern ocean (Pagani et al., 2011), and pCO<sub>2</sub> (ppm) alkenone-based from ODP  
1321 925 (white circles; Pagani et al., 2011; Zhang et al., 2013), ODP 929 (black circles; Pagani et al.,  
1322 2011), and pCO<sub>2</sub> boron isotope-based from TDP17/12 (grey triangles; Pearson et al., 2009) are also  
1323 shown. For comparison with sea surface temperature (SST) proxies, the Mg/Ca (mmol/mol; Peck et  
1324 al., 2010) at Site 1263 and the SST from U<sup>k</sup><sub>37</sub> at low latitude in the Atlantic Ocean (Liu et al., 2009)  
1325 are also displayed. The positions of EOB and Step 2 at Site 1263 are reported.

1326

1327 **Figure 6.** Paleoproductivity indices from nannofossil (PC2) and benthic foraminifer ( $\Delta\delta^{13}\text{C}_{\text{P-B}}$   
1328 calculated from data in Riesselman et al. (2007) and Peck et al. (2010); Fisher's alpha index -  
1329 diversity proxy, extinction group species, phytodetritus-using species, buliminid species and the  
1330 species *Nuttalides umbonifera*) datums are plotted against depth. The positions of EOB and Step 2  
1331 are reported.

1333

Table 1

Datum	This study Interval (hole-core-section, cm)	Depth (mcd)	Shipboard Scientific Party (Zachos et al., 2004)	Age (Ma)	Ages References
			Average Depth (mcd)		
T <i>Isthmolithus recurvus</i>	B-3H-5, 115-116	83.19	86	32.7	Lyle et al. (2002)
T <i>Coccolithus formosus</i>	A-9H-4, 9-10	85.16	86	32.92	Pälike et al. (2006)
Bc <i>Sphenolithus akropodus</i>	A-9H-4, 100-102	86.34	N.A.		
B <i>Chiasmolithus altus</i>	B-4H-2, 131-132	89.4	N.A.	33.31*	Pälike et al. (2006)
B <i>Sphenolithus akropodus</i>	B-4H-3, 50-52	90.09	N.A.		
Bc <i>Clausicoccus subdistichus</i>	A-10H-4, 141-142	96.92	94.77	33.88*	Pälike et al. (2006)
T <u><i>Hantkenina</i> spp.</u>	A-10H-5, 32-34/B-4H, CC	97.53	104.5	33.89	Gradstein et al. (2012)
<u><i>Pseudohastigerina</i> size reduction</u>	A-10H-5, 32-34/B-4H, CC	97.53	N.A.	33.89	Gradstein et al. (2012)
T <u><i>Turborotalia cerroazulensis</i> group</u>	A-10H-5, 32-34/B-4H, CC	97.53	N.A.		
T <i>Discoaster saipanensis</i>	B-5H-3, 50-52	102.27	104.1	34.44	Pälike et al. (2006)
T <i>Discoaster barbadiensis</i>	B-5H-4, 0-2	103.27	N.A.	34.77	Pälike et al. (2006)
B <i>Sphenolithus tribulosus</i>	B-5H-4, 50-52	103.77	N.A.		

Fig. 1

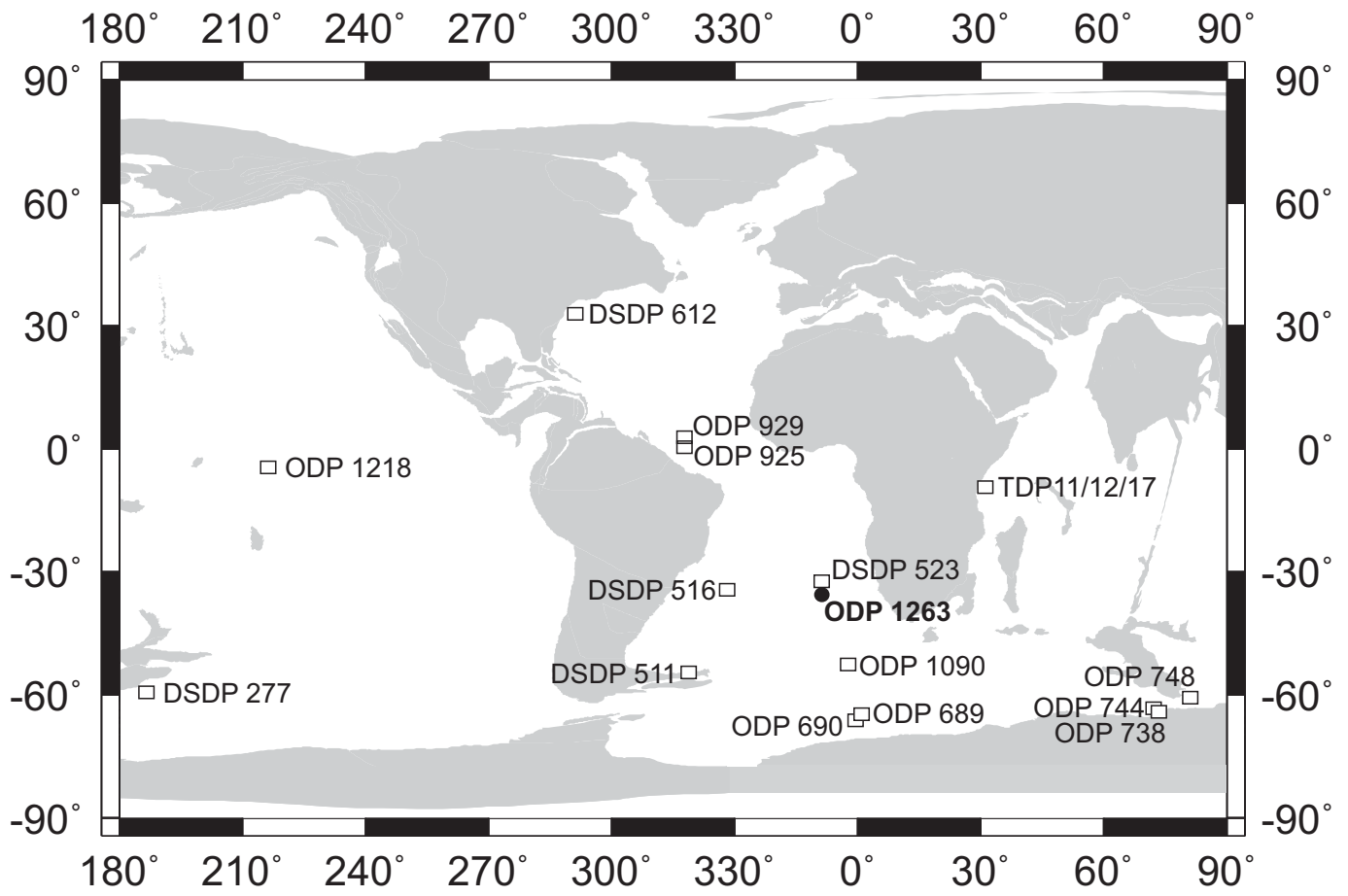


Fig. 2

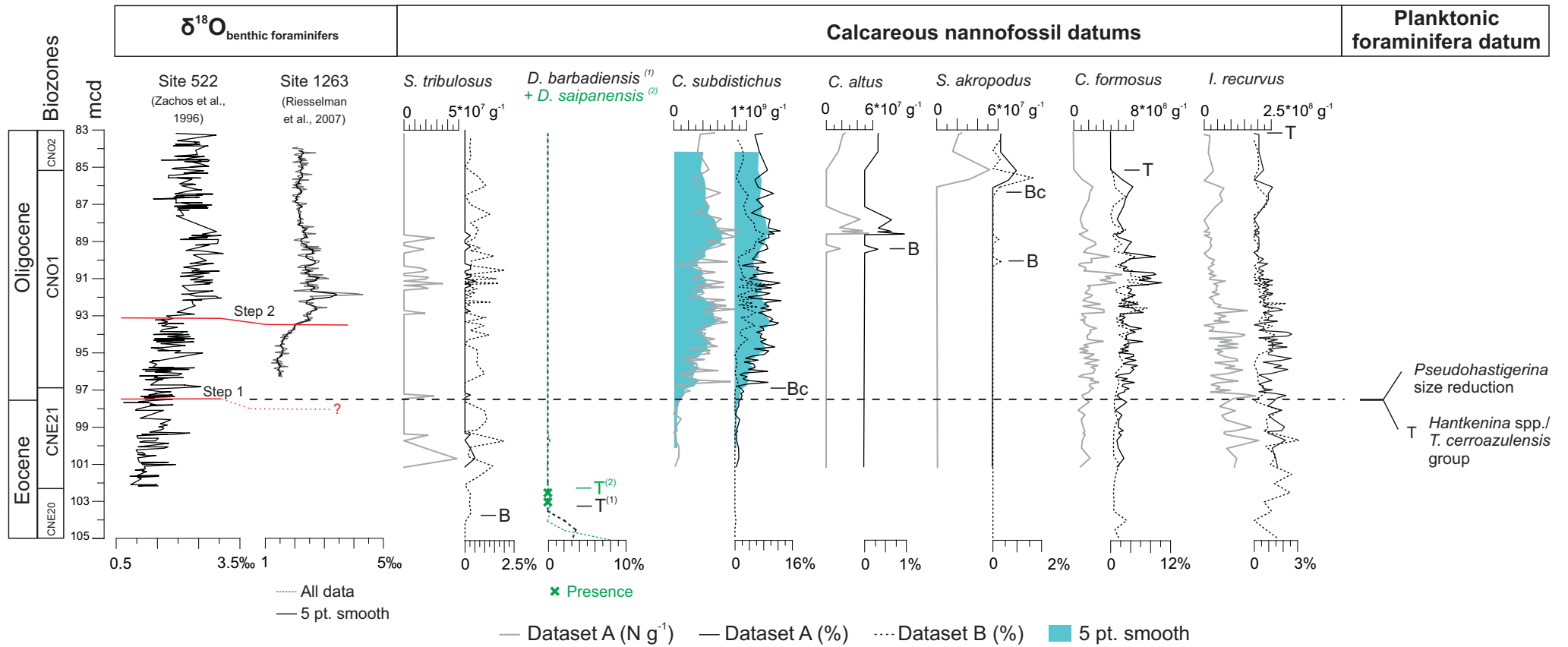


Fig. 3

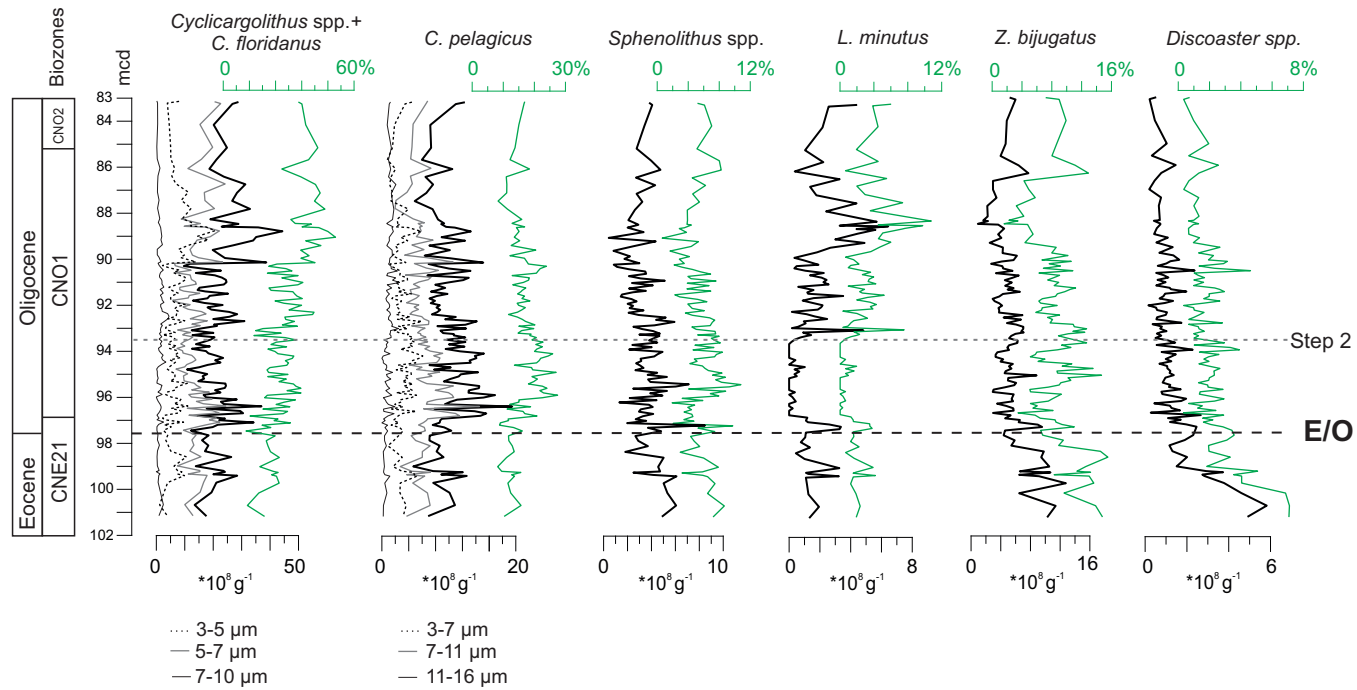
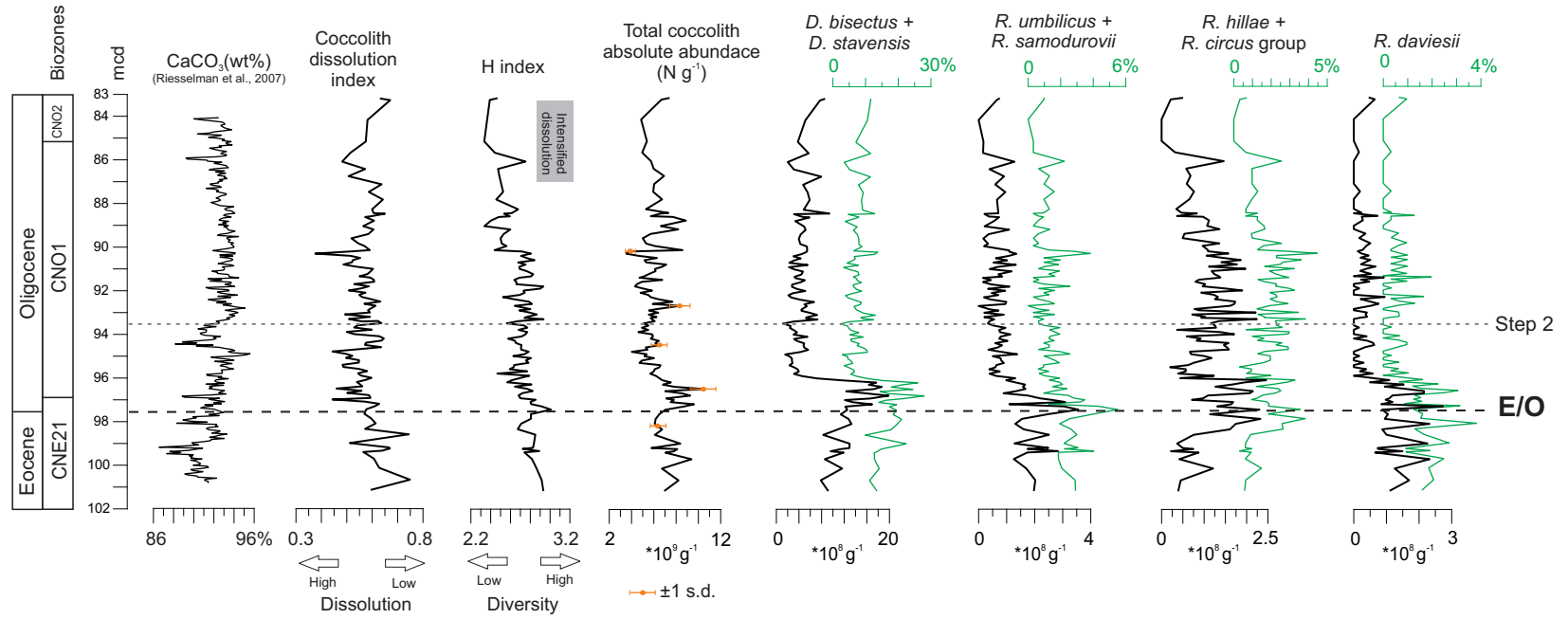
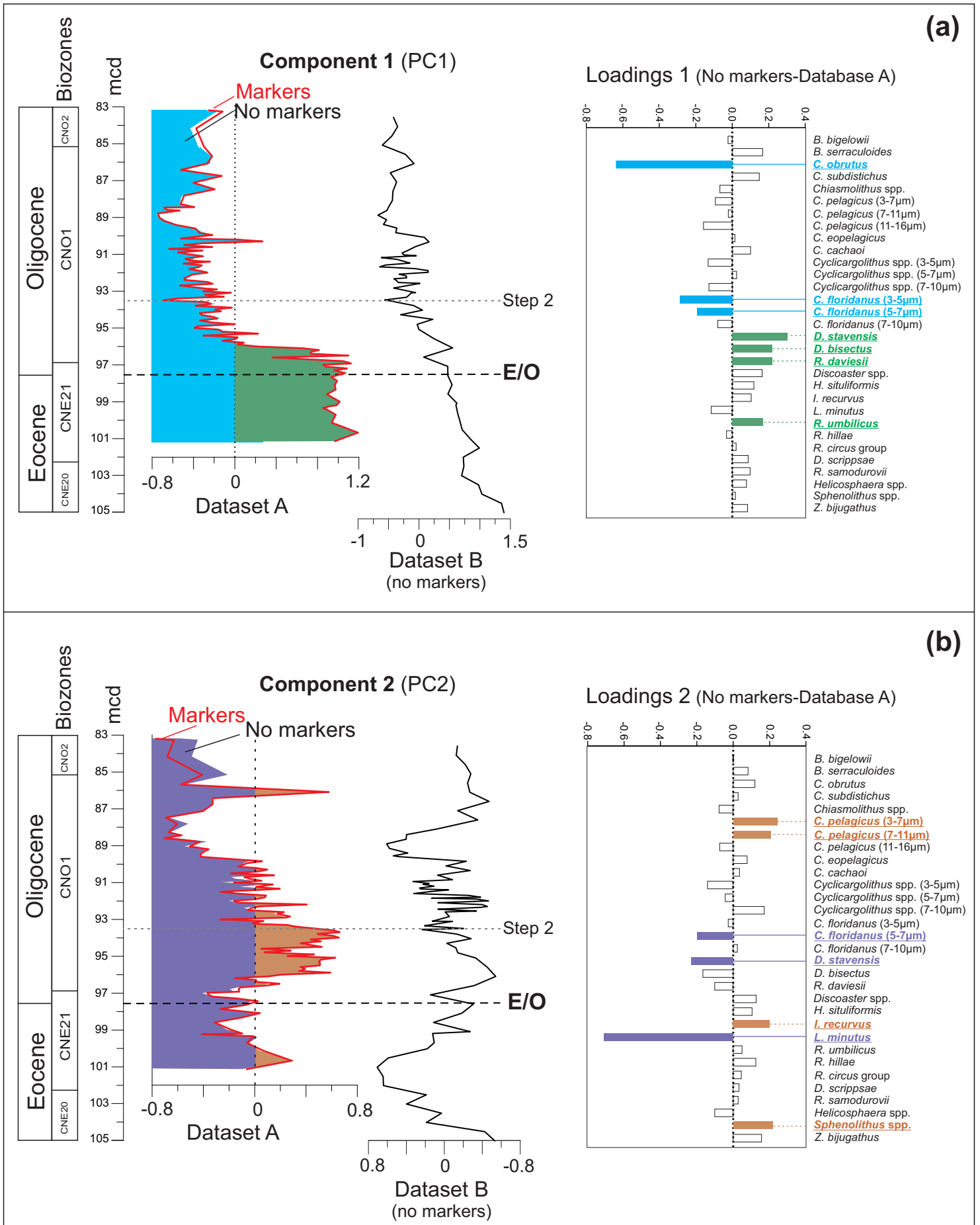


Fig. 4



# Fig. 5

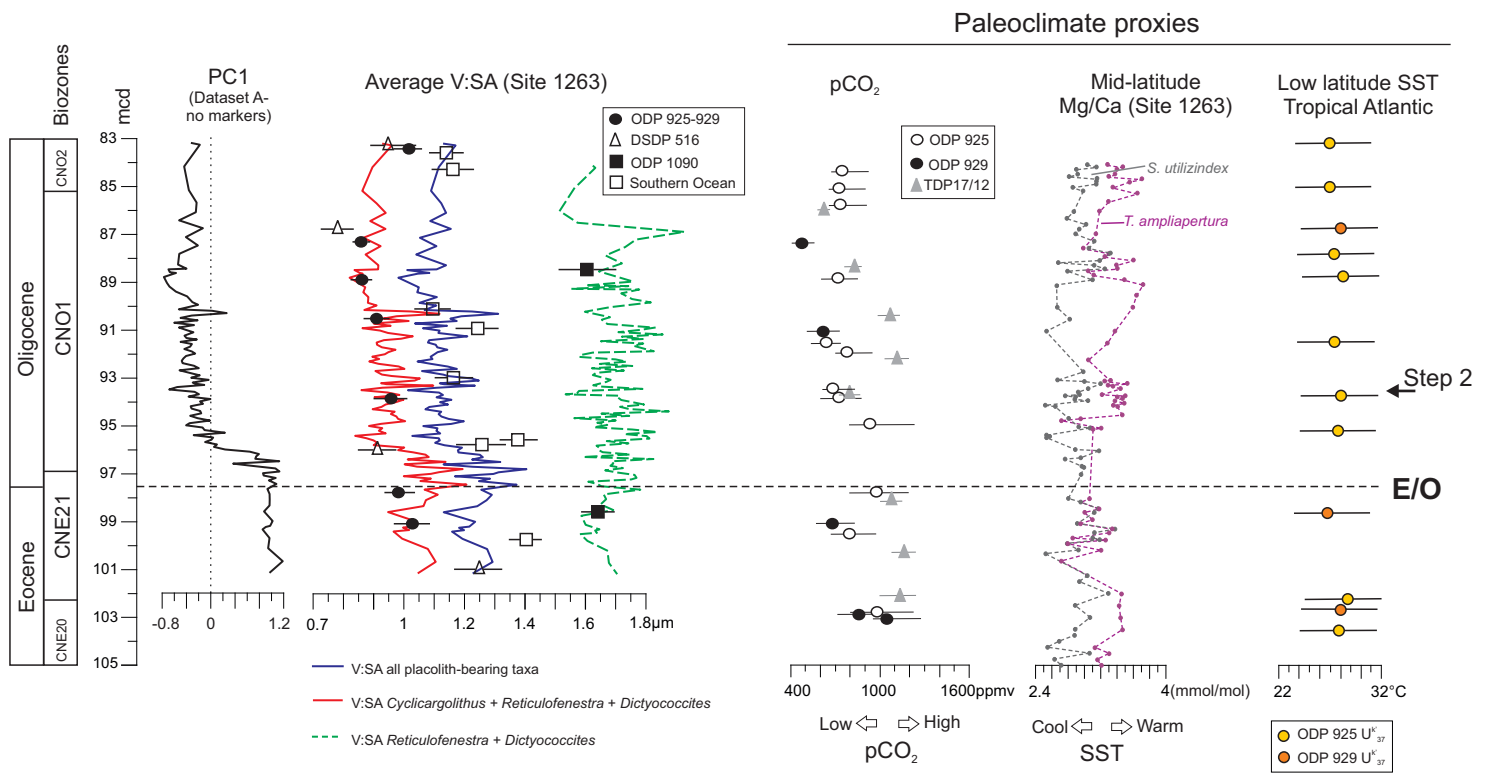


Fig. 6

